

Wind-Induced Changes to Surface Gravity Wave Shape in Deep to Intermediate Water

Thomas Zdyrski¹†, and Falk Feddersen¹

¹ Scripps Institution of Oceanography, UCSD, La Jolla, CA 92092-0209, USA

(Received xx; revised xx; accepted xx)

Wave shape (*i.e.* skewness or asymmetry) plays an important role in beach morphology evolution, remote sensing, and ship safety. Wind's influence on ocean waves has been extensively studied theoretically in the context of growth, but most theories are phase averaged and cannot predict wave shape. Most laboratory and numerical studies similarly focus on wave growth. A few laboratory experiments have demonstrated that wind can change wave shape, and two-phase numerical simulations have also noted wind-induced wave shape changes. However, wind's effect on wave shape is poorly understood, and no theory for it exists. For weakly nonlinear waves, wave shape parameters are the phase of the harmonic relative to the primary frequency (or harmonic phase HP, zero for a Stokes wave) and relative amplitude of the harmonic to the primary. Here, surface pressure profiles (denoted Jeffreys, Miles, and Generalized Miles) are prescribed based on wind-wave generation theories. Theoretical solutions are derived for quasi-periodic progressive waves and the wind-induced changes to HP, relative harmonic amplitude, as well as already known phase speed changes and growth rates. The wave shape parameters depend upon the chosen surface pressure profile, pressure magnitude and phase relative to the wave profile, and the nondimensional depth. Wave asymmetry is linked to the nondimensional growth rate. Atmospheric large eddy simulations constrain pressure profile parameters. HP predictions are qualitatively consistent with laboratory observations. This theory, together with the observables of HP and relative harmonic amplitude, can provide insight into the actual wave surface pressure profile.

1. Introduction

The shape of surface gravity waves plays a role in many physical phenomena. Wave shape is described by the third-order statistical moments, skewness and asymmetry (*e.g.* Hasselmann 1962; Elgar *et al.* 1990). These two parameters are integral in determining sediment transport direction (onshore *vs.* offshore) and magnitude (*e.g.* Drake & Calantoni 2001; Hsu & Hanes 2004; Gonzalez-Rodriguez & Madsen 2007), which play key roles in beach morphodynamics (*e.g.* Hoefel & Elgar 2003; Grasso *et al.* 2011). Wave shape is also pertinent in remote sensing, where wave skewness modulates the returned waveform in radar altimetry (*e.g.* Jackson 1979; Hayne 1980; Huang *et al.* 1983) and wave asymmetry affects the thermal emissions measured in polarimetric radiometry (*e.g.* Kunkee & Gasiewski 1997; Piepmeier & Gasiewski 2001; Johnson & Cai 2002). Additionally, these wave shape plays a role in determining ship response to wave impacts (*e.g.* Soares *et al.* 2008; Oberhagemann *et al.* 2013). Waves propagating on a flat bottom are ordinarily symmetric, though a number of processes can create asymmetry. While some wave asymmetry inducing-phenomena, such as wave shoaling (*e.g.*

† Email address for correspondence: tzdyrski@physics.ucsd.edu

Elgar & Guza 1985, 1986), are well understood, the effect of wind on wave shape is still poorly understood.

The influence of wind on ocean waves has been extensively studied, although primarily in the context of wave growth. An initial investigation by Jeffreys (1925) was based on a sheltering hypothesis where separated airflow resulted in reduced pressure on the leeward side of the wave, causing wave growth. While conceptually simple, this mechanism fell out of favour because such separation only occurs near breaking (Banner & Melville 1976) and is therefore unlikely to contribute meaningfully to wave growth (Young 1999). However, Jeffreys's theory has inspired some recent work: Belcher & Hunt (1993) developed a fully turbulent model wherein the sheltering effect causes a thickening of the boundary layer and wave growth, even without separation. Later treatments utilized different physical mechanisms such as resonant forcing by incoherent, turbulent eddies (Phillips 1957), vortex forcing from vertically sheared airflow (*e.g.* Miles 1957; Lighthill 1962), and non-separated sheltering (*e.g.* Belcher & Hunt 1993). Janssen (2004) provides an extensive overview of the relevant developments in wind-wave generation theory. When deriving energy and momentum fluxes from air to water, all of these seminal theories on wave growth (*e.g.* Phillips 1957; Lighthill 1962; Belcher & Hunt 1993) utilized a phase-averaging technique, which removes wave-shape information. Thus, although these theories of wind-wave interaction focused on the wave growth rate, no theoretical work has investigated the effect of wind on wave shape in a physically consistent manner.

Measurements and numerical simulations have also been used to investigate the dependence of wave growth on wind speed. Field measurements (*e.g.* Longuet-Higgins 1962; Snyder 1966; Hasselmann *et al.* 1973) and laboratory experiments (*e.g.* Shemdin & Hsu 1967; Plant & Wright 1977; Mitsuyasu & Honda 1982) have been used to parameterize how quickly intermediate and deep-water waves grow under various wind conditions, including short fetch (*e.g.* Lamont-Smith & Waseda 2008) and strong wind conditions (*e.g.* Troitskaya *et al.* 2012). Note, direct measurements of wave surface pressure (related to growth) are notoriously difficult (*e.g.* Donelan *et al.* 2005). Similarly, numerical simulations have also been used to predict wind-induced growth rates. Early atmospheric numerical models used the Reynolds-averaged Navier Stokes equations (RANS, *e.g.* Gent & Taylor 1976; Al-Zanaidi & Hui 1984) to calculate the energy loss of the wind field, however these early simulations could only approximate turbulence through a Reynolds-averaging process. Recent studies have analysed the turbulence behaviour in detail. Particle image velocimetry (PIV) and laser-induced fluorescence (LIF) have been used for turbulence measurements in laboratory experiments and have revealed turbulent structures above the waves (*e.g.* Veron *et al.* 2007; Buckley & Veron 2017, 2019). This turbulent behaviour has also been captured through direct numerical simulations (DNS) of the governing equations (*e.g.* Yang & Shen 2009, 2010) and by parameterizing subgrid-scale processes in large eddy simulations (LES, *e.g.* Yang *et al.* 2013; Hara & Sullivan 2015; Hao *et al.* 2018). When solving for the atmospheric dynamics, many of these simulations prescribe a static sinusoidal wave shape while focusing on the evolution of the wind field, as well as energy and momentum transfers. Therefore, any wind-induced changes to wave shape were not captured.

While there has been much research regarding wind-induced wave growth, wave shape has seen relatively little work. Two-phase (air and water) numerical simulations have begun incorporating dynamically evolving waves into their analyses (*e.g.* Liu *et al.* 2010; Xuan *et al.* 2016; Deike *et al.* 2017; Hao & Shen 2019). These studies directly model the evolution of both the air and wave fields in a coupled manner, no longer prescribing a fixed wave shape (*e.g.* Hara & Sullivan 2015; Hao *et al.* 2018). Furthermore, some also qualitatively consider how wave shape evolves under the influence of wind (*e.g.*

Yan & Ma 2010; Xie 2014, 2017). However, these analyses are focused on other parameters and do not quantify precisely how the wave shape changes. Additionally, there have been a small number of field measurements (*e.g.* Cox & Munk 1956) and laboratory experiments (Feddersen & Veron 2005; Leykin *et al.* 1995) that have directly investigated how wind affects wave shape. It was found that the skewness and asymmetry depended on wind speed for mechanically-generated waves in relatively deep (Leykin *et al.* 1995) or intermediate and shallow (Feddersen & Veron 2005) water. In particular, the wave asymmetry (Leykin *et al.* 1995), skewness (Cox & Munk 1956) and energy ratio of the first harmonic (frequency $2f$) to the primary (frequency f) (Feddersen & Veron 2005) all increased with wind speed. It would be beneficial to develop a theory that can explain these experimental findings.

In this paper, we develop a theory coupling wind to dynamically evolving intermediate and deep-water waves ($kh \geq 1$ with k the wavenumber and h the water depth). We consider the fluid domain beneath a periodic, progressive wave that is forced by a prescribed, wave-dependent surface pressure profile. That is, the atmosphere is not treated dynamically. The wind effect on wave shape requires a nonlinear theory. As the surface boundary conditions for gravity waves are nonlinear, the equations are solved using a multiple scales perturbation analysis where the wave steepness $\varepsilon := a_1 k$ (with a_1 the amplitude of the primary wave) is small and new, slower timescales are introduced over which the nonlinearities act (see, for example Mei *et al.* 2005). This formalism has been used to derive the canonical Stokes waves, which are periodic, progressive waves of permanent form in intermediate and deep water (Stokes 1880). By introducing a surface pressure forcing term, we will allow for solutions of the form

$$\eta = a_1 e^{i(kx - \omega t)} + a_2 e^{i[2(kx - \omega t) + \beta]} + \dots, \quad (1.1)$$

with the real part is implied. Here η is the wave height, ω is the wave frequency, and $a_1 k = \varepsilon$ and $a_2 k = O(\varepsilon^2)$ are the nondimensional amplitudes of the primary and first harmonic, respectively. We have defined a new parameter, the ‘‘harmonic phase’’ (or HP) β , which is analogous to the biphase, a statistical tool (Elgar & Guza 1985). The wave shape (*i.e.*, skewness and asymmetry) are functions of HP β and relative harmonic amplitude $a_2/(a_1^2 k)$. For example, both skewness and asymmetry are zero for $a_2/(a_1^2 k) = 0$, and asymmetry is zero for $\beta = 0$. For a deep-water ($kh \gg 1$) Stokes wave without wind forcing, $\omega = \sqrt{g/k}(1 + \frac{1}{2}a_1^2)$ with g the acceleration due to gravity, $a_2/(a_1^2 k) = \frac{1}{2}$ giving a non-zero skewness, and $\beta = 0$ yielding no phase difference between the harmonics in (1.1). Indeed, unforced Stokes waves are exactly symmetric at all orders (Toland 2000).

Three surface pressure profiles, derived from the theories of Jeffreys (1925) and Miles (1957), are included in the perturbation expansion. Using the method of multiple-scales, Stokes wave-like solutions are derived, giving the wave shape (via $a_2/(a_1^2 k)$ and β) dependence on the wind-induced surface pressure profile. Additionally, wave growth will result from the fact that $\text{Im}\{\omega\}$ is no longer zero (*e.g.* Miles 1957). These solutions reduce to the unforced Stokes waves when the pressure forcing vanishes.

In section 2, we set up the equations and define the different pressure profiles used. Section 3 begins the general derivation covering a range of realistic pressure magnitudes, which is continued in appendix A. A key aspect to the derivation (section 3 and appendix A), we include the nondimensional pressure p' in the leading-order equations ($p' = O(\varepsilon)$) which is the most nuanced, but also allows the formal replacement $p' \rightarrow \varepsilon p'$ or $p' \rightarrow \varepsilon^2 p'$, generating the weaker $p' = O(\varepsilon^2)$ and $p' = O(\varepsilon^3)$ solutions (appendix A.5). In section 4, we discuss the results of this analysis. Section 5 details the relevance of these findings and connects them to existing studies. Appendix A extends the general

derivation to higher orders in ε to demonstrate a weak amplitude dependence of the shape parameters.

2. Theoretical Background

2.1. Governing Equations

Here, we specify the equations governing the water dynamics, Homogeneous, incompressible fluids satisfy the incompressible continuity equation

$$\nabla \cdot \vec{u} = 0,$$

within the fluid. We assume irrotational flow, allowing the water velocity \vec{u} to be written in terms of a velocity potential as $\vec{u} = \nabla\phi$. We define a coordinate system with $z = 0$ at the mean water level, positive z upwards, and gravity pointing in the $-z$ direction. We assume planar wave propagation in the $+x$ direction and uniform in the y direction. Then, the incompressibility condition becomes Laplace's equation:

$$\frac{\partial^2\phi}{\partial x^2} + \frac{\partial^2\phi}{\partial z^2} = 0. \quad (2.1)$$

Assuming water of uniform depth with a flat bottom located at $z = -h$, we impose a no-flow bottom boundary condition

$$\frac{\partial\phi}{\partial z} = 0 \quad \text{at} \quad z = -h. \quad (2.2)$$

Finally, the standard surface boundary conditions (*e.g.* Whitham 2011) are the kinematic boundary condition,

$$w = \frac{\partial\eta}{\partial t} + \vec{u} \cdot \nabla\eta \quad \text{at} \quad z = \eta, \quad (2.3)$$

and the dynamic boundary condition

$$0 = \frac{p}{\rho_w} + g\eta + \frac{\partial\phi}{\partial t} + \frac{1}{2} \left(\frac{\partial\phi^2}{\partial x} + \frac{\partial\phi^2}{\partial z} \right) \quad \text{at} \quad z = \eta, \quad (2.4)$$

with $\eta(x, t)$ the surface profile and $p(x, t)$ the surface pressure evaluated at $z = \eta$. In section 2.3 we specify the surface pressure profiles.

2.2. Assumptions

Our analysis is characterized by a number of nondimensional parameters. The wave slope $\varepsilon := a_1 k$, assumed small, will order our perturbation expansion. Additionally, we will restrict our attention to intermediate and deep water by requiring that the nondimensional depth $kh \geq O(1)$ so that the Ursell parameter is small, $\varepsilon/(kh)^3 \ll 1$. An additional parameter is the nondimensional surface pressure magnitude induced by the wind discussed in sections 2.3 and 2.4. We seek waves with wavelength $\lambda := 2\pi/k$ travelling in the x direction that are periodic in x and quasi-periodic in t :

$$\eta(x, t) = \eta(x + \lambda, t) = \eta(\theta, t) \quad \text{and} \quad \phi(x, z, t) = \phi(x + \lambda, z, t) = \phi(\theta, z, t), \quad (2.5)$$

with θ defined in (A 66) and analogous to the standard $kx - \text{Re}\{\omega\}t$. Additionally, we neglect the surface tension σ by restricting to wavelengths $\lambda \gg 2$ cm implying a large Bond number ($\rho g/k^2\sigma \gg 1$). Furthermore, we assume no mean Eulerian current. Finally, we seek only primary waves and their bound harmonics as solutions.

In the dynamic boundary condition (2.4), we incorporated the normal stress (surface

pressure) but neglected the shear stress, as the normal stress is usually significantly larger than the shear stress (*e.g.* Kendall 1970; Hara & Sullivan 2015; Husain *et al.* 2019). Additionally, we note that surface shear stresses cause a slight thickening of the boundary layer, which is equivalent to a pressure phase shift on the remainder of the water column (Longuet-Higgins 1969). Therefore, we can include the effect of shear stresses through a phase shift in the pressure relative to the wave profile. Hence, in this investigation we only consider pressures acting normal to the wave surface.

The irrotational assumption was motivated by our assumption that vorticity-generating wind shear stresses are small; additionally, any such vorticity is constrained to a thin boundary layer just below the surface of the waves (Longuet-Higgins 1969). Finally, viscous forces vanish—necessary for Bernoulli’s equation (2.4)—for any flow that is both irrotational and incompressible (with constant viscosity; *e.g.* Fang 2019). Thus, we will assume irrotational, inviscid flow throughout the fluid interior.

2.3. Surface Pressure Profiles

Here, we define the surface pressure profiles used in the analysis. The Jeffreys (1925) theory yields a (“Jeffreys”) surface pressure profile,

$$p_J(x, t) = s\rho_a U^2 \frac{\partial \eta(x, t)}{\partial x}, \quad (2.6)$$

with $\eta(x, t)$ the surface profile, ρ_a the air density, U a characteristic wind speed, and s an empirical, unitless, order-1 constant. In contrast, the Miles (1957) theory of wind-wave growth gives a (“Miles”) surface pressure profile of the form

$$p_M(x, t) = \left(\tilde{\alpha} + i\tilde{\beta} \right) \rho_a U^2 k \eta_a(x, t), \quad (2.7)$$

with $\tilde{\alpha}$ and $\tilde{\beta}$ empirical, unitless, order-1 constants, k the wavenumber, and η_a the analytic representation[†] of η .

Miles’s theory was developed for a single sinusoidal wave profile without harmonics. Although naively applying (2.7) to a multi-harmonic (*e.g.* Stokes) wave is permitted, another suitable generalization, which captures the motivation behind the Miles profile, is specifying the wind as leading or trailing η . Thus, we define another (“Generalized Miles”) surface pressure profile as

$$p_G(x, t) = r\rho_a U^2 k \eta(kx + \psi_P, t), \quad (2.8)$$

with r a new, unitless, order-1 constant, and the new parameter, the “wind phase” ψ_P , corresponds to the phase shift between the wave and the pressure profile. As the surface pressure is elevated on the windward (relative to leeward) side of the wave, $\psi_P > 0$ corresponds to wind blowing from the left, assuming $\psi_P \in (-\pi, \pi)$.

To facilitate comparison, the various pressure profiles are written in a common form. Inspired by similarities in (2.6) to (2.8), we define a non-negative pressure magnitude constant, P , which implicitly encodes the wind speed:

$$P \propto \rho_a U^2. \quad (2.9)$$

Our analysis will be agnostic regarding the U dependence. The form specified in (2.9) only serves as motivation. Since $k\|\eta\|_2 = O(\varepsilon)$ ($\|\cdot\|_2$ is the L_2 norm), we see can from

[†] The analytic representation of a real function $f(x)$ is $f(x) + i\hat{f}(x)$ with $\hat{f}(x)$ the Hilbert transform of $f(x)$. For our purposes, only two representations will be relevant: the analytic representation of $\cos(x)$ is e^{ix} and that of $\sin(x)$ is $-ie^{ix}$.

the various definitions (2.6) to (2.8) that

$$O(\|p\|_2) = O(\varepsilon P). \quad (2.10)$$

For instance, we will define P_J for Jeffreys the profile such that

$$p_J(x, t) = P_J e^{i\psi_P} \frac{\partial \eta(x, t)}{\partial x}, \quad (2.11)$$

with $\psi_P = \pm \frac{1}{2}\pi$. Likewise, we will rewrite the Miles and Generalized Miles profiles as

$$p_M(x, t) = P_M e^{i\psi_P} k \eta_a(x, t). \quad (2.12)$$

$$p_G(x, t) = P_G k \eta(kx + \psi_P, t). \quad (2.13)$$

These three surface ($z = \eta$) pressure profiles, (2.11) to (2.13), are expanded in a Fourier series to yield simpler equations. Expanding arbitrary functions $f(x)$ in Fourier series as the real part of $f(x) = \sum_{m=0} \hat{f}_m \exp(imkx)$ with $m \in \mathbb{N}$ yields

$$\hat{p}_{J,m}(t) = \pm i k m P_J \hat{\eta}_m(t), \quad (2.14)$$

$$\hat{p}_{M,m}(t) = k P_M e^{i \operatorname{sgn} m \psi_P} \hat{\eta}_m(t), \quad (2.15)$$

$$\hat{p}_{G,m}(t) = k P_G e^{i m \psi_P} \hat{\eta}_m(t). \quad (2.16)$$

Therefore, we will generically write

$$\hat{p}_m(t) = k \hat{P}_m \hat{\eta}_m(t), \quad (2.17)$$

with $\hat{P}_m = m P_J e^{i\psi_P}$ and $\psi_P = \pm \frac{1}{2}\pi$ for Jeffreys, $\hat{P}_m = P_M e^{i \operatorname{sgn} m \psi_P}$ for Miles, and $\hat{P}_m = P_G e^{i m \psi_P}$ for Generalized Miles profiles. Note, the wind phase ψ_P is a free parameter for the Miles and Generalized Miles profiles. Thus, by appropriate choice of \hat{P}_m , we can represent surface pressures as convolutions of $\eta(x, t)$ with arbitrary (time-independent) functions of x .

To make these definitions concrete, and to contrast the different forcing types, a deep-water, second-order Stokes wave profile

$$k\eta = \varepsilon \cos \theta + \frac{1}{2} \varepsilon^2 \cos 2\theta \quad (2.18)$$

is shown for $\varepsilon = 0.2$ (fig. 1a). The Stokes wave profile is used to express the three (unity normalized) surface pressure profiles (fig. 1b), where $\psi_P = \pi/2$ is chosen for Miles and Generalized Miles profiles. These three pressure profiles, (2.11) to (2.13), are largely similar to each other, although differences arise due to the Stokes wave harmonics. The derivative in the Jeffreys profile (blue fig. 1b) multiplies each Fourier component by its wavenumber, mk , enhancing higher frequencies. The wind phase ψ_P , measured left from $\theta = 0$ to the pressure maximum, shifts the entire pressure waveform relative to the surface waveform η for the Generalized Miles profile (orange fig. 1b). Contrast this to the Miles profile (green fig. 1b), where ψ_P shifts the phase of the m -th Fourier component by ψ_P/m radians, distorting the waveform η . The LES numerical simulations of Hara & Sullivan (2015) and Husain *et al.* (2019) show $\psi_P \approx 3\pi/4$ for a variety of wind speeds (section 5.1). However, in fig. 1, each surface pressure profile is depicted for $\psi_P = \frac{1}{2}\pi$ to facilitate comparison with the Jeffreys case (for which $\psi_P = \pm \frac{1}{2}\pi$).

2.4. Determination of Pressure Magnitude P

We use existing experimental data to determine the magnitude of P in various contexts. Assuming a logarithmic wind profile, Miles (1957) derived the wave-energy growth rate

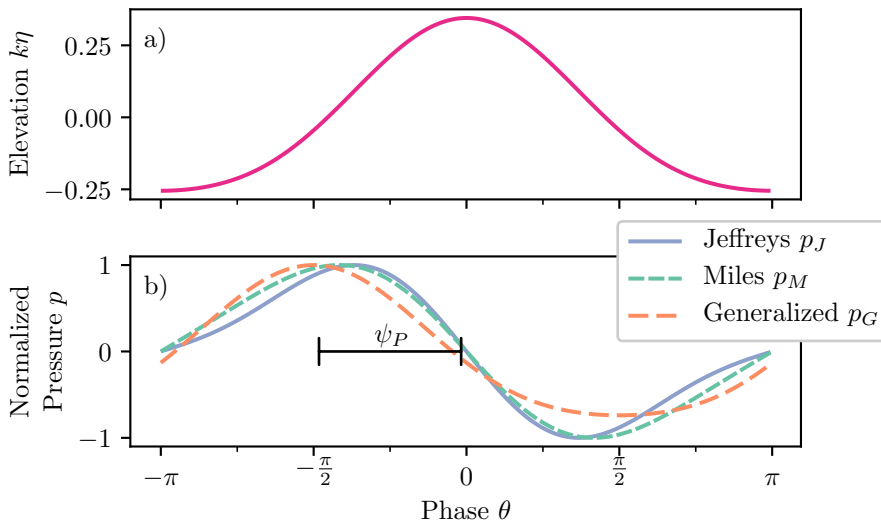


Figure 1. (Colour online) (a) Nondimensional, right-propagating Stokes wave $k\eta$ (2.18) as a function of phase $\theta = kx - \omega t$ with $\varepsilon = 0.2$. (b) Normalized surface pressure profiles $p(\theta)$ as described in (2.11) to (2.13); see legend. The maximum pressure magnitude is normalized to unity (arbitrary units), and a value of $\psi_P = \frac{1}{2}\pi$ was chosen to facilitate comparison with the Jeffreys profile with ψ_P positive corresponding to wind blowing to the right.

γ , normalized by the (unforced, linear, deep-water) wave frequency f_0^∞ , for the pressure profile p_M (2.12):

$$\frac{\gamma}{f_0^\infty} = 2\pi\tilde{\beta}\frac{\rho_a}{\rho_w}\frac{U^2k}{(c_0^\infty)^2} = 2\pi\frac{P_M}{\rho_w(c_0^\infty)^2}\sin\psi_P, \quad (2.19)$$

where, $c_0^\infty = \sqrt{g/k}$ is the linear, deep-water phase speed, ρ_w is the water density, and (2.9) is used to define P_M . Using the value $\psi_P = 3\pi/4$ from Hara & Sullivan (2015) and Husain *et al.* (2019) gives $P_M k/(\rho_w g) = 0.23(\gamma/f_0^\infty)$.

Furthermore, we use empirical data relating wind speed U to growth rate to constrain the P_M pressure magnitude constant in deep-water. Figure 2 shows the energy growth rate γ/f_0^∞ as a function of inverse wave age, u_*/c_0^∞ with u_* the friction velocity. The empirical observations of deep-water γ/f_0^∞ versus u_*/c_0^∞ collapse onto a curve permitting a conversion from u_*/c_0^∞ to γ/f_0^∞ , yielding $P_M k/(\rho_w g)$ (2.19).

Here, we consider $\|p\|_2 k/(\rho_w g) = O(\varepsilon)$ to $O(\varepsilon^3)$, or $Pk/(\rho_w g) = O(1)$ to $O(\varepsilon^2)$. If we assume $\varepsilon \approx 0.1$ and $\psi_P \approx 3\pi/4$, then (2.19) shows we are considering growth rates $\gamma/f_0^\infty \approx 4 \times 10^{-2}$ to 4. Referring to fig. 2, we see these reside mostly in the laboratory measurement regime, corresponding to $u_*/c_0^\infty \approx 5 \times 10^{-1}$ to 5. We can approximate U_{10} using the standard logarithmic boundary layer theory (*e.g.* Monin & Obukhov 1954):

$$u_* = \frac{\kappa U_{10}}{\ln[(10\text{ m})/z_0]}, \quad (2.20)$$

with $\kappa \approx 0.4$ the von Kármán constant and $z_0 \approx 2.1 \times 10^{-4}$ the surface roughness parameter for 2 m long, 0.1 m high deep-water waves, as one might have in a wave

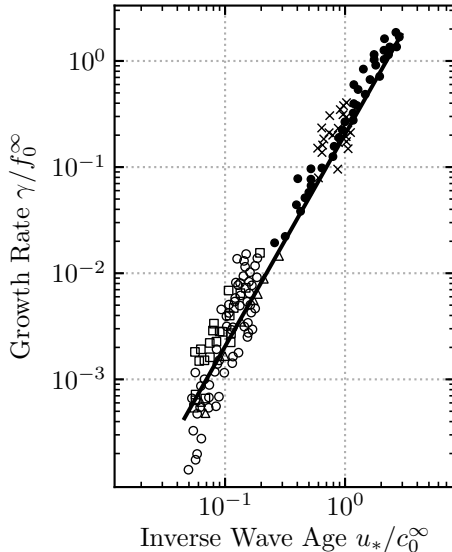


Figure 2. Nondimensional, deep-water wave-energy growth rate γ/f_0^∞ versus inverse wave age, u_*/c_0^∞ with u_* the wind's friction velocity and $c_0^\infty = \sqrt{g/k}$ the linear, deep-water phase speed. The filled symbols represent laboratory measurements while the hollow symbols represent field measurements (from Komen *et al.* 1994). The solid line represents the fit parameterized by Banner & Song (2002).

tank (Taylor & Yelland 2001). Substituting the values, we find

$$U_{10} \approx 27u_*, \quad (2.21)$$

yielding $U_{10}/c_0^\infty \approx 10^1$ to 10^2 , or $U_{10} \approx 3 \times 10^1 \text{ m s}^{-1}$ to $3 \times 10^2 \text{ m s}^{-1}$ assuming a deep-water dispersion relation.

It is interesting to examine the pressure forcing magnitude used previously. Phillips (1957) modelled wave growth using a different mechanism than considered here where the pressure forcing was included at the same order as η . That is, $\|p\|_2 k/(\rho_w g) = O(\varepsilon)$, or $Pk/(\rho_w g) = O(1)$. Referring to fig. 2, this corresponded to strongly forced waves and fast wind ($u_*/c_0^\infty = O(1)$). Other theoretical works have often chosen $\|p\|_2 k/(\rho_w g) = O(\varepsilon^2)$ (e.g. Janssen 1982; Brunetti *et al.* 2014; Brunetti & Kasparian 2014) or $\|p\|_2 k/(\rho_w g) = O(\varepsilon^3)$ (e.g. Kharif *et al.* 2010; Leblanc 2007; Onorato & Proment 2012). Thus, the choices of $Pk/(\rho_w g) = O(1)$ to $O(\varepsilon^2)$ are all relevant in the literature.

2.5. Nondimensionalization

Nondimensional systems are useful in perturbation expansions. Here, a standard nondimensionalization (e.g. Mei *et al.* 2005) is performed, defining new nondimensional, order-1 primed variables:

$$\begin{aligned} x &= \frac{x'}{k}, & z &= \frac{z'}{k}, & \eta &= \varepsilon \frac{\eta'}{k}, \\ t &= \frac{t'}{\sqrt{gk}}, & h &= \frac{h'}{k}, & \Phi &= \varepsilon \Phi' \sqrt{\frac{g}{k^3}}, \end{aligned} \quad (2.22)$$

Notice the factor of ε in the equations for η and ϕ , since these are assumed small. Unlike in the standard Stokes wave problem, the surface pressure must also be nondimensionalized. As show in (2.10), $O(\|p\|_2) = \varepsilon O(P)$. Thus, we find p and P (as well as their Fourier transforms) are nondimensionalized by

$$(p, \hat{p}) = O\left(\frac{\varepsilon P k}{\rho_w g}\right) \frac{\rho_w g}{k} (p', \hat{p}'), \quad (2.23)$$

$$(P, \hat{P}_m) = O\left(\frac{P k}{\rho_w g}\right) \frac{\rho_w g}{k} (P', \hat{P}'_m), \quad (2.24)$$

with $p'(x, t)$ and P' (as well as their Fourier transforms) now order-unity and dimensionless. For the remainder of the paper, primes will be dropped and all variables will be assumed nondimensional and order-unity, except where explicitly stated.

3. Derivation of Wave Shape Parameters

We now couple a prescribed surface pressure profile (2.17) to the nonlinear wave problem (2.1) to (2.4) to derive the wind's effect on wave shape. The end result will be an expression for the nondimensional surface profile of the form

$$\eta = \varepsilon A_1(t_1, \dots) e^{i(x - \omega_0 t_0)} + \varepsilon^2 A_2(t_1, \dots) e^{2i(x - \omega_0 t_0) + \beta} + \dots, \quad (3.1)$$

where the real part is implied. A comparison of nondimensional (3.1) with dimensional (1.1) shows we will have (ignoring the time-dependence; *cf.* appendix A.4) $a_1 = \varepsilon A_1$, $a_2 = \varepsilon^2 A_2/k$, *etc.*, so $A_2/A_1^2 = a_2/(a_1^2 k)$. Both the HP β and a_2/a_1^2 encode information about the wave shape. We take the ratio a_2/a_1^2 because we will find that $a_2 \propto \exp(2 \operatorname{Im}\{\omega_0\} t_0)$ while $a_1 \propto \exp(\operatorname{Im}\{\omega_0\} t_0)$. As we are mainly interested in the shape, the growth is removed by using the ratio a_2/a_1^2 .

Expanding our nondimensional variables in an asymptotic series of ε , we have

$$\begin{aligned} \eta &= \sum_{n=1}^{\infty} \varepsilon^n \eta_n(x, t_0, t_1, \dots), \\ \phi &= \sum_{n=1}^{\infty} \varepsilon^n \phi_n(x, z, t_0, t_1, \dots), \\ p &= \sum_{n=1}^{\infty} \varepsilon^n p_n(x, t_0, t_1, \dots). \end{aligned}$$

Recall that the nondimensional pressure forcing can enter at different orders depending on the wind strength (*cf.* section 2.4). Here and in appendix A, we include pressure in the leading-order equations ($Pk/(\rho_w g) = O(1)$, *i.e.* $p_1 \neq 0$) which is the most nuanced, but also allows the formal replacement $P \rightarrow \varepsilon P$ or $P \rightarrow \varepsilon^2 P$ generating $Pk/(\rho_w g) = O(\varepsilon)$ and $Pk/(\rho_w g) = O(\varepsilon^2)$ solutions (appendix A.5). Here, we solve the equations to $O(\varepsilon^2)$, giving the leading order contribution to our shape parameters, β and $a_2/(a_1^2 k)$. In appendix A, we solve the equations to $O(\varepsilon^4)$, yielding the next non-zero correction to the shape parameters (demonstrating a weak amplitude dependence).

Laplace's equation (2.1) is solved via a Fourier transform and, with the bottom boundary condition (2.2), has solution (real part implied)

$$\phi_n(x, z, t_0, t_1, \dots) = \frac{\cosh[m(z+h)]}{\sinh(mh)} e^{imx} \hat{\phi}_{n,m}(t_0, t_1, \dots), \quad (3.2)$$

with arbitrary $m \in \mathbb{N}$ and arbitrary function $\hat{\phi}_{n,m}(t_0, t_1, \dots)$. Furthermore, to express the surface pressure profile p_n in terms of the surface height η_n (cf. (2.17)), all variables are written as a Fourier series:

$$\eta_n(x, t_0, t_1, \dots) = \sum_{m=0}^{m=n} e^{imx} \hat{\eta}_{n,m}(t_0, t_1, \dots) \quad (3.3)$$

$$\phi_n(x, z, t_0, t_1, \dots) = \sum_{m=0}^{m=n} e^{imx} \hat{\phi}_{n,m}(t_0, t_1, \dots) \frac{\cosh(m(z+h))}{\sinh(mh)}, \quad (3.4)$$

$$p_n(x, t_0, t_1, \dots) = \sum_{m=0}^{m=n} e^{imx} \hat{p}_{m,n}(t_0, t_1, \dots). \quad (3.5)$$

Aside from the pressure expansion, this follows the standard Stokes expansion methodology (e.g. Mei *et al.* 2005; Ablowitz 2011). Recall that we previously related (cf. (2.17)) the Fourier-transform of the surface pressure to the surface profile,

$$\hat{p}_{m,n}(t_0, t_1, \dots) = \hat{P}_m \hat{\eta}_{m,n}(t_0, t_1, \dots). \quad (3.6)$$

Thus, the pressure has higher-order corrections because η has higher-order Stokes-like corrections.

We now expand the kinematic (2.3) and dynamic (2.4) boundary conditions in ε and collect terms order-by-order.

$O(\varepsilon)$:

$$\frac{\partial \eta_1}{\partial t_0} - \frac{\partial \phi_1}{\partial z} = 0 \quad (3.7)$$

$$\eta_1 + \frac{\partial \phi_1}{\partial t_0} + p_1 = 0, \quad (3.8)$$

$O(\varepsilon^2)$:

$$\frac{\partial \phi_2}{\partial z} - \frac{\partial \eta_2}{\partial t_0} = \frac{\partial \eta_1}{\partial t_1} + \frac{\partial \eta_1}{\partial x} \frac{\partial \phi_1}{\partial x} - \eta_1 \frac{\partial^2 \phi_1}{\partial z^2}, \quad (3.9)$$

$$\eta_2 + \frac{\partial \phi_2}{\partial t_0} + p_2 = -\frac{\partial \phi_1}{\partial t_1} - \eta_1 \frac{\partial \phi_1}{\partial z \partial t_0} - \frac{1}{2} \left(\frac{\partial \phi_1}{\partial x} \right)^2 - \frac{1}{2} \left(\frac{\partial \phi_1}{\partial z} \right)^2, \quad (3.10)$$

$O(\varepsilon^3)$:

$$\frac{\partial \phi_3}{\partial z} - \frac{\partial \eta_3}{\partial t_0} = \frac{\partial \eta_2}{\partial t_1} + \frac{\partial \eta_1}{\partial t_2} + \frac{\partial \eta_2}{\partial x} \frac{\partial \phi_1}{\partial x} + \frac{\partial \eta_1}{\partial x} \frac{\partial \phi_2}{\partial x} + \eta_1 \frac{\partial \eta_1}{\partial x} \frac{\partial^2 \phi_1}{\partial z \partial x} - \eta_1 \frac{\partial^2 \phi_2}{\partial z^2} \quad (3.11)$$

$$\begin{aligned} & - \frac{1}{2} \eta_1^2 \frac{\partial^3 \phi_1}{\partial z^3} - \eta_2 \frac{\partial^2 \phi_1}{\partial z^2}, \\ \eta_3 + \frac{\partial \phi_3}{\partial t_0} + p_3 = & -\frac{\partial \phi_1}{\partial t_2} - \frac{\partial \phi_2}{\partial t_1} - \frac{1}{2} \eta_1^2 \frac{\partial^3 \phi_1}{\partial z^2 \partial t_0} - \eta_1 \frac{\partial^2 \phi_2}{\partial z \partial t_0} - \eta_2 \frac{\partial^2 \phi_1}{\partial z \partial t_0} \\ & - \eta_1 \frac{\partial^2 \phi_1}{\partial z \partial t_1} - \frac{\partial \phi_1}{\partial x} \frac{\partial \phi_2}{\partial x} - \eta_1 \frac{\partial \phi_1}{\partial x} \frac{\partial^2 \phi_1}{\partial x \partial z} - \frac{\partial \phi_1}{\partial z} \frac{\partial \phi_2}{\partial z} - \eta_1 \frac{\partial \phi_1}{\partial z} \frac{\partial^2 \phi_1}{\partial z^2}, \end{aligned} \quad (3.12)$$

$O(\varepsilon^4)$:

$$\begin{aligned}
\frac{\partial \phi_4}{\partial z} - \frac{\partial \eta_4}{\partial t_0} = & -\frac{\partial \eta_1}{\partial t_3} - \frac{\partial \eta_2}{\partial t_2} - \frac{\partial \eta_3}{\partial t_1} - \frac{\partial \eta_1}{\partial x} \frac{\partial \phi_3}{\partial x} - \frac{\partial \eta_2}{\partial x} \frac{\partial \phi_2}{\partial x} - \frac{\partial \eta_3}{\partial x} \frac{\partial \phi_1}{\partial x} + \eta_3 \frac{\partial^2 \phi_1}{\partial z^2} \\
& - \left(\frac{\partial \eta_1}{\partial x} \frac{\partial^2 \phi_1}{\partial x \partial z} - \frac{\partial^2 \phi_2}{\partial z^2} \right) \eta_2 - \left(\frac{\partial \eta_1}{\partial x} \frac{\partial^2 \phi_2}{\partial x \partial z} + \frac{\partial \eta_2}{\partial x} \frac{\partial^2 \phi_1}{\partial x \partial z} - \frac{\partial^2 \phi_3}{\partial z^2} \right) \eta_1 + \frac{\partial^3 \phi_1}{\partial z^3} \eta_1 \eta_2 \\
& - \left(\frac{1}{2} \frac{\partial \eta_1}{\partial x} \frac{\partial^2 \phi_1}{\partial x \partial z} - \frac{1}{2} \frac{\partial^3 \phi_2}{\partial z^3} \eta_1^2 - \frac{1}{6} \frac{\partial^4 \phi_1}{\partial z^4} \eta_1^3 \right),
\end{aligned} \tag{3.13}$$

$$\begin{aligned}
\eta_4 + \frac{\partial \phi_4}{\partial t_0} + p_4 = & -\frac{\partial \phi_1}{\partial t_3} - \frac{\partial \phi_2}{\partial t_2} - \frac{\partial \phi_3}{\partial t_1} - \frac{\partial \phi_1}{\partial x} \frac{\partial \phi_3}{\partial x} - \frac{1}{2} \left(\frac{\partial \phi_2}{\partial x} \right)^2 - \frac{\partial \phi_1}{\partial z} \frac{\partial \phi_3}{\partial z} \\
& - \frac{1}{2} \left(\frac{\partial \phi_2}{\partial z} \right)^2 - \frac{\partial^2 \phi_1}{\partial t_0 \partial z} \eta_3 - \left(\frac{\partial^2 \phi_1}{\partial t_1 \partial z} + \frac{\partial^2 \phi_2}{\partial t_0 \partial z} + \frac{\partial \phi_1}{\partial x} \frac{\partial^2 \phi_1}{\partial x \partial z} + \frac{\partial \phi_1}{\partial z} \frac{\partial^2 \phi_1}{\partial z^2} \right) \eta_2 \\
& - \left(\frac{\partial^2 \phi_1}{\partial t_2 \partial z} + \frac{\partial^2 \phi_2}{\partial t_1 \partial z} + \frac{\partial^2 \phi_3}{\partial t_0 \partial z} + \frac{\partial \phi_1}{\partial x} \frac{\partial^2 \phi_2}{\partial x \partial z} + \frac{\partial \phi_2}{\partial x} \frac{\partial^2 \phi_1}{\partial x \partial z} + \frac{\partial \phi_1}{\partial z} \frac{\partial^2 \phi_2}{\partial z^2} + \frac{\partial \phi_2}{\partial z} \frac{\partial^2 \phi_1}{\partial z^2} \right) \eta_1 \\
& - \frac{\partial^2 \phi_1}{\partial t_0 \partial z} \eta_1 \eta_2 - \left(\frac{1}{2} \frac{\partial^2 \phi_1}{\partial t_1 \partial z} + \frac{1}{2} \frac{\partial^2 \phi_2}{\partial t_0 \partial z} + \frac{1}{2} \frac{\partial \phi_1}{\partial x} \frac{\partial^2 \phi_1}{\partial x \partial z} + \frac{1}{2} \left(\frac{\partial^2 \phi_1}{\partial x \partial z} \right)^2 + \frac{1}{2} \frac{\partial \phi_1}{\partial z} \frac{\partial^3 \phi_1}{\partial z^3} \right. \\
& \left. + \frac{1}{2} \left(\frac{\partial^2 \phi_1}{\partial z^2} \right)^2 \right) \eta_1^2 - \frac{1}{6} \frac{\partial^2 \phi_1}{\partial t_0 \partial z} \eta_1^3.
\end{aligned} \tag{3.14}$$

We solve these equations to $O(\varepsilon^2)$ here and leave the solution of $O(\varepsilon^4)$ equations to appendix A.

3.1. $O(\varepsilon)$ Equations

Here, we assume the pressure enters the leading order equations with $Pk/(\rho_w g) = O(1)$. Proceeding to first-order in ε , the linearised boundary conditions are

$$\begin{aligned}
\frac{\partial \phi_1}{\partial z} - \frac{\partial \eta_1}{\partial t_0} &= 0, \\
\frac{\partial \phi_1}{\partial t_0} + \eta_1 + p_1 &= 0.
\end{aligned}$$

Inserting the Fourier transforms (3.3) to (3.5) and substituting the pressure profile (2.17) gives

$$\begin{aligned}
\hat{\phi}_{1,1} - \frac{\partial \hat{\eta}_{1,1}}{\partial t_0} &= 0, \\
\frac{\partial \hat{\phi}_{1,1}}{\partial t_0} \coth(h) + \hat{\eta}_{1,1} + \hat{P}_1 \hat{\eta}_{1,1} &= 0.
\end{aligned}$$

Combining equations to eliminate $\hat{\eta}_{1,1}$ gives

$$\frac{\partial^2 \hat{\phi}_{1,1}}{\partial t_0^2} \coth(h) + \left(1 + \hat{P}_1 \right) \hat{\phi}_{1,1} = 0. \tag{3.15}$$

This is the usual, finite depth, linear operator on $\hat{\phi}_{1,1}$ modified by the presence of \hat{P}_1 , showing that $\hat{\phi}_{1,1}(t_0, t_1, \dots)$ is harmonic. Using a bit of foresight to define the constants, we write

$$\hat{\phi}_{1,1} = -i\omega_0 A_1 e^{-i\omega_0 t_0}, \quad (3.16)$$

giving

$$\phi_1 = -i\omega_0 A_1 e^{i(x-\omega_0 t_0)} \frac{\cosh(z+h)}{\sinh(h)}, \quad (3.17)$$

where

$$\omega_0 = \pm \sqrt{\tanh(h) \left(1 + \hat{P}_1\right)}. \quad (3.18)$$

The (+) sign corresponds to waves propagating to the right. Inserting this into the surface boundary conditions gives equations for η_1 ,

$$\frac{\partial \hat{\eta}_1}{\partial t_0} = -i\omega_0 A_1(t_1) e^{-i\omega_0 t_0}, \quad (3.19)$$

$$\hat{\eta}_1 + \hat{P}_1 \hat{\eta}_1 = \coth(h) \omega_0^2 A_1(t_1) e^{-i\omega_0 t_0} \quad (3.20)$$

This gives

$$\eta_1 = A_1 e^{i(x-\omega_0 t_0)}, \quad (3.21)$$

with ω_0 given above.

It is instructive to consider the real and imaginary parts of ω_0 :

$$\text{Re}\{\omega_0\} = \pm \sqrt{\frac{\tanh(h)}{2}} \sqrt{1 + \text{Re}\{\hat{P}_1\} + \sqrt{1 + |\hat{P}_1|^2 + 2 \text{Re}\{\hat{P}_1\}}}, \quad (3.22)$$

$$\text{Im}\{\omega_0\} = \pm \text{sgn}\left(\text{Im}\{\hat{P}_1\}\right) \sqrt{\frac{\tanh(h)}{2}} \sqrt{-1 - \text{Re}\{\hat{P}_1\} + \sqrt{1 + |\hat{P}_1|^2 + 2 \text{Re}\{\hat{P}_1\}}}. \quad (3.23)$$

Notice that the pressure causes growth ($\text{Im}\{\omega_0\} > 0$) for wind in the direction of the waves ($\text{sgn}[\text{Im}\{\hat{P}_1\}] = \text{sgn}[\text{Re}\{\omega_0\}]$) and decay ($\text{Im}\{\omega_0\} < 0$) for opposing wind ($\text{sgn}[\text{Im}\{\hat{P}_1\}] = -\text{sgn}[\text{Re}\{\omega_0\}]$). Likewise, observe that an applied pressure, $\hat{P}_1 \neq 1$, modifies the dispersion relation (3.22). This phenomena was also derived by Jeffreys (1925) and Miles (1957) for $Pk/(\rho_w g) = O(\varepsilon)$, which we can reproduce by formally taking $\hat{P}_1 \rightarrow \varepsilon \hat{P}_1$ in (3.22) and (3.23).

3.2. $O(\varepsilon^2)$ Equations

Proceeding to second-order, the kinematic and dynamic boundary conditions are

$$\frac{\partial \phi_2}{\partial z} - \frac{\partial \eta_2}{\partial t_0} = \frac{\partial \eta_1}{\partial t_1} + \frac{\partial \eta_1}{\partial x} \frac{\partial \phi_1}{\partial x} - \eta_1 \frac{\partial^2 \phi_1}{\partial z^2}, \quad (3.24)$$

$$\frac{\partial \phi_2}{\partial t_0} + \eta_2 + p_2 = -\frac{\partial \phi_1}{\partial t_1} - \eta_1 \frac{\partial^2 \phi_1}{\partial z \partial t_0} - \frac{1}{2} \left(\frac{\partial \phi_1}{\partial x} \right)^2 - \frac{1}{2} \left(\frac{\partial \phi_1}{\partial z} \right)^2. \quad (3.25)$$

By taking Fourier transforms (3.3) to (3.5), we can express p_2 using (3.6). Inserting the first-order solutions and collecting harmonics yields

$m = 1$ Fourier Component:

$$\hat{\phi}_{2,1} - \frac{\partial \hat{\eta}_{2,1}}{\partial t_0} = \frac{\partial A_1}{\partial t_1} e^{-i\omega_0 t_0}, \quad (3.26)$$

$$\frac{\partial \hat{\phi}_{2,1}}{\partial t_0} \coth(h) + (1 + \hat{P}_1) \hat{\eta}_{2,1} = i\omega_0 \frac{\partial A_1}{\partial t_1} e^{-i\omega_0 t_0} \coth(h). \quad (3.27)$$

$m = 2$ Fourier Component:

$$2\hat{\phi}_{2,2} - \frac{\partial \hat{\eta}_{2,2}}{\partial t_0} = i\omega_0 A_1^2 e^{-2i\omega_0 t_0} \coth(h), \quad (3.28)$$

$$\frac{\partial \hat{\phi}_{2,2}}{\partial t_0} \coth(2h) + (1 + \hat{P}_2) \hat{\eta}_{2,2} = \frac{1}{4} \omega_0^2 A_1^2 e^{-2i\omega_0 t_0} (2 - \operatorname{csch}^2(h)). \quad (3.29)$$

$m = 0$ Fourier Component:

$$-\frac{\partial \hat{\eta}_{2,0}}{\partial t_0} = 0, \quad (3.30)$$

$$\frac{\partial \hat{\phi}_{2,0}}{\partial t_0} + \hat{\eta}_{2,0} = \frac{1}{2} \left(2 \operatorname{Re}\{\omega_0^2\} - |\omega_0|^2 (2 + \operatorname{csch}^2(h)) \right) |A_1|^2 |e^{-i\omega_0 t_0}|^2. \quad (3.31)$$

Eliminating the various $\hat{\eta}_{2,m}$ to get equations solely in terms of $\hat{\phi}_{2,m}$ gives

$m = 1$ Fourier Component:

$$\frac{\partial^2 \hat{\phi}_{2,1}}{\partial t_0^2} \coth(h) + (1 + \hat{P}_1) \hat{\phi}_{2,1} = 2 \left(1 + \hat{P}_1 \right) \frac{\partial A_1}{\partial t_1} e^{-i\omega_0 t_0}. \quad (3.32)$$

$m = 2$ Fourier Component:

$$\begin{aligned} \frac{\partial^2 \hat{\phi}_{2,2}}{\partial t_0^2} \coth(2h) + 2(1 + \hat{P}_2) \hat{\phi}_{2,2} = & -i \frac{1}{2} \omega_0 A_1^2 \left\{ [2 - \operatorname{csch}^2(h)] \omega_0^2 \right. \\ & \left. - 2(1 + \hat{P}_2) \coth(h) \right\} e^{-2i\omega_0 t_0}. \end{aligned} \quad (3.33)$$

$m = 0$ Fourier Component:

$$\frac{\partial^2 \hat{\phi}_{2,0}}{\partial t_0^2} = \left(2\omega_0^2 - |\omega_0|^2 (2 + \operatorname{csch}^2(h)) \right) |A_1|^2 e^{2 \operatorname{Im}\{\omega_0\} t_0} \operatorname{Im}\{\omega_0\}. \quad (3.34)$$

Preventing secular terms in $\hat{\phi}_{2,1}$ requires that $\partial_{t_1} A_1 = 0$. Solving this for $\hat{\phi}_{2,m}$ and transforming back to ϕ_2 via (3.2) gives

$$\begin{aligned} \phi_2 = & i \frac{\omega_0}{4} A_1^2 \coth(h) \frac{(2 - \operatorname{csch}^2(h)) \omega_0^2 - 2 \left[1 + \hat{P}_2 \right] \coth(h)}{(2 + \operatorname{csch}^2(h)) \omega_0^2 - \left[1 + \hat{P}_2 \right] \coth(h)} e^{2i(x - \omega_0 t_0)} \frac{\cosh[2(z + h)]}{\sinh(2h)} \\ & + \frac{1}{8 \operatorname{Im}\{\omega_0\}} \left(2\omega_0^2 - |\omega_0|^2 (2 + \operatorname{csch}^2(h)) \right) |A_1|^2 \left(e^{2 \operatorname{Im}\{\omega_0\} t_0} - 1 \right). \end{aligned} \quad (3.35)$$

We've included a constant term -1 in $\exp(2 \operatorname{Im}\{\omega_0\} t_0) - 1$ so that ϕ_2 remains finite if $P \rightarrow 0$ (*i.e.* $\operatorname{Im}\{\omega_0\} \rightarrow 0$). We have also dropped the homogeneous solution, which would only amount to redefining the linear solution, A_1 .

The surface boundary conditions give equations for η_2 :

$$\frac{\partial \hat{\eta}_2}{\partial t_0} = -i \frac{1}{2} \omega_0^3 A_1^2 e^{2i(x-\omega_0 t_0)} \frac{(2 + 3 \operatorname{csch}^2(h)) \coth(h)}{(2 + \operatorname{csch}^2(h)) \omega_0^2 - [1 + \hat{P}_2] \coth(h)} \quad (3.36)$$

$$[1 + \hat{P}_2] \hat{\eta}_2 = \frac{1}{4} [1 + \hat{P}_2] A^2 e^{2i(x-\omega_0 t_0)} \frac{(2 + 3 \operatorname{csch}^2(h)) \coth(h) \omega_0^2}{(2 + \operatorname{csch}^2(h)) \omega_0^2 - [1 + \hat{P}_2] \coth(h)} \quad (3.37)$$

These have the solution

$$\eta_2 = \frac{1}{4} A_1^2 e^{2i(x-\omega_0 t_0)} (2 + 3 \operatorname{csch}^2(h)) \coth(h) \left(1 - \coth^2(h) \left[\frac{\hat{P}_2 - \hat{P}_1}{1 + \hat{P}_1} \right] \right)^{-1} \quad (3.38)$$

Redimensionalizing, we find

$$\eta = \varepsilon \frac{A_1}{k} e^{i(x-\omega_0 t_0)} + \varepsilon^2 \frac{A_1^2}{k} e^{2i(x-\omega_0 t_0)} C_{2,2} + O(\varepsilon^3), \quad (3.39)$$

where we have defined $C_{2,2}$ as

$$C_{2,2} := \frac{1}{4} (2 + 3 \operatorname{csch}^2(h)) \coth(h) \left(1 - \coth^2(h) \left[\frac{\hat{P}_2 - \hat{P}_1}{1 + \hat{P}_1} \right] \right)^{-1}. \quad (3.40)$$

Note that $A_1^2 |C_{2,2}|/k$ is the quantity we called A_2 in (3.1).

We have now found the primary $\hat{\eta}_{m=1} = \varepsilon \hat{\eta}_{1,m} + O(\varepsilon^3)$ and first harmonic $\hat{\eta}_{m=2} = \varepsilon^2 \hat{\eta}_{2,2} + O(\varepsilon^3)$. Therefore, the amplitudes of the primary and harmonics are respectively

$$a_1 := |\hat{\eta}_{m=1}| = \varepsilon \frac{|A_1(t_2)|}{k} e^{\operatorname{Im}\{\omega_0\}t_0} + O(\varepsilon^3), \quad (3.41)$$

$$a_2 := |\hat{\eta}_{m=2}| = \varepsilon^2 \frac{|A_1^2(t_2)|}{k} e^{2 \operatorname{Im}\{\omega_0\}t_0} |C_{2,2}| + O(\varepsilon^3). \quad (3.42)$$

Hence, in order to cancel the t_0 -dependence, we define the relative harmonic amplitude shape parameter as

$$\frac{a_2}{a_1^2 k} := \left| \frac{\hat{\eta}_{m=2}}{\hat{\eta}_{m=1}^2 k} \right|. \quad (3.43)$$

With this definition, (3.39) becomes

$$\eta = a_1 e^{i(x - \operatorname{Re}\{\omega_0\}t_0)} + \frac{a_2}{a_1^2 k} e^{2i(x - \operatorname{Re}\{\omega_0\}t_0) + \beta} + O(\varepsilon^3), \quad (3.44)$$

where we have defined the harmonic phase β as the complex angle of $\hat{\eta}_{m=2}/\hat{\eta}_{m=1}^2$:

$$\beta := \tan^{-1} \left(\frac{\operatorname{Im}\{\hat{\eta}_{m=2}/\hat{\eta}_{m=1}^2\}}{\operatorname{Re}\{\hat{\eta}_{m=2}/\hat{\eta}_{m=1}^2\}} \right). \quad (3.45)$$

In general, both β and $a_2/(a_1^2 k)$ will have an expansion in ε since $\hat{\eta}_{m=2}$ will have higher-order corrections. For instance, the HP β has expansion $\beta = \beta_0 + \varepsilon \beta_1 + \dots$. Inserting our

solution (3.39) into (3.45) gives β_0 , which is just the complex angle of $C_{2,2}$ at this order:

$$\begin{aligned}\beta_0 &= \tan^{-1} \left(\frac{\operatorname{Im} \left\{ \left[\frac{\hat{P}_2 - \hat{P}_1}{1 + \hat{P}_1} \right] \right\}}{\tanh^2(h) - \operatorname{Re} \left\{ \left[\frac{\hat{P}_2 - \hat{P}_1}{1 + \hat{P}_1} \right] \right\}} \right) \\ &= \tan^{-1} \left(\frac{\operatorname{Im} \left\{ \left[\hat{P}_2 - \hat{P}_1 \right] \left(1 + \hat{P}_1^* \right) \right\}}{\left| 1 + \hat{P}_1 \right|^2 \tanh^2(h) - \operatorname{Re} \left\{ \left[\hat{P}_2 - \hat{P}_1 \right] \left(1 + \hat{P}_1^* \right) \right\}} \right),\end{aligned}\quad (3.46)$$

with a asterisk representing the complex conjugate. Similarly, using (3.43) shows that the leading order term of $a_2/(a_1^2 k)$ is just $|C_{2,2}|$ to this order:

$$\frac{a_2}{a_1^2 k} = |C_{2,2}| = \frac{2 + 3 \operatorname{csch}^2(h)}{4} \coth(h) \left| 1 - \coth^2(h) \left[\frac{\hat{P}_2 - \hat{P}_1}{1 + \hat{P}_1} \right] \right|^{-1}. \quad (3.47)$$

Without wind ($\hat{P}_1 = \hat{P}_2 = 0$), $C_{2,2}$ reduces to $\frac{1}{4}(2 + 3 \operatorname{csch}^2(h)) \coth(h)$, or $\frac{1}{2}$ in deep water. This reproduces the usual, Stokes waves values of $a_2/(a_1^2 k) = \frac{1}{2}$ in deep water and $\beta \rightarrow 0$. By solving the kinematic and dynamic boundary conditions to $O(\varepsilon^2)$ we have generated the leading-order terms for β and $a_2/(a_1^2 k)$. Note that these are also converted to the wave skewness and asymmetry in appendix A.3. We continue this analysis by solving to $O(\varepsilon^4)$ in appendix A, deriving the first non-trivial correction and demonstrating a weak time- and amplitude-dependence to the shape parameters.

4. Results

Now, we present the main results of this theory. The harmonic phase β , harmonic coefficients a_1 and a_2 , and complex frequency ω depend on the four nondimensional parameters: the wave steepness $\varepsilon := a_1 k$, the water depth kh , the pressure magnitude constant $Pk/(\rho_w g)$, and the wind phase ψ_P . To reduce the nondimensional parameter range, we keep a fixed $\varepsilon = 0.1$. Recall (section 2.2) the requirement of $\varepsilon/(kh)^3 \leq 1$, such that the expansion remains properly ordered, implies $kh \geq 0.5$, though we keep $kh \geq 1$. Note that taking kh to ∞ yields solutions on infinite depth. The pressure magnitude constant P is P_J , P_M , or P_G corresponding to the choice of pressure profile. For each solution, taking $P \rightarrow 0$ recovers the unforced Stokes wave.

For the remainder of the paper, we will revert to dimensional variables. In particular, the pressure constant P is dimensional again and not necessarily order-1. Replacing the multiple timescales with the true time t in our solution (3.44), we obtain (*cf.* section 3) a surface height profile η of the form (A 67)

$$k\eta = (a_1 k) e^{i\theta} + (a_1 k)^2 \frac{a_2}{a_1^2 k} e^{2i\theta + \beta} + \dots, \quad (4.1)$$

with the real part implied. Here, θ is defined in (A 66) and is analogous to the standard $kx - \operatorname{Re}\{\omega\}t$ with $\omega(t) = \omega_0 + \varepsilon\omega_1(t) + \dots$ the full, time-dependent frequency (A 60) and waves propagating to the right for $\operatorname{Re}\{\omega\} > 0$. On the other hand, the wind blows from the left if $\psi_P > 0$, assuming $\psi_P \in (-\pi, \pi)$. Note that the growth of the harmonics means the perturbation expansion is liable to become disordered after a long time. Therefore, these solutions are only valid for finite time.

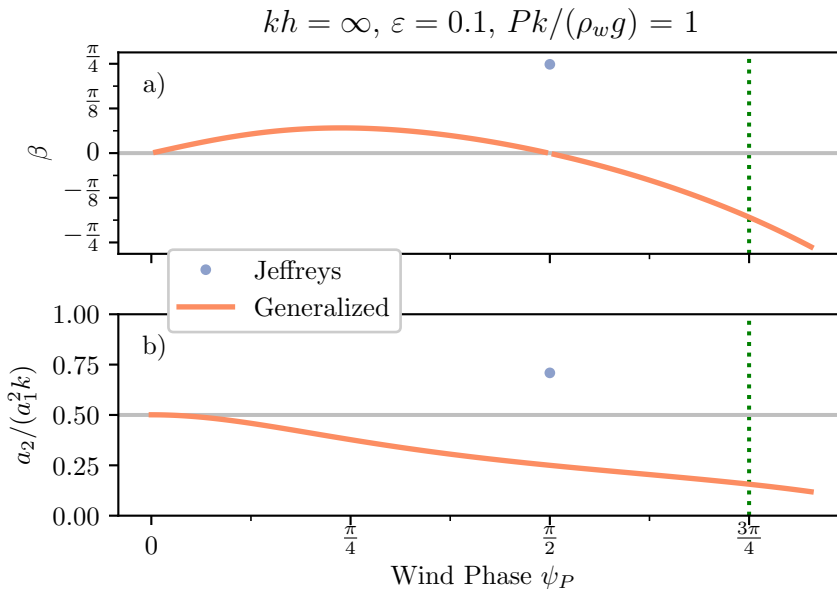


Figure 3. (Colour online) (a) Harmonic phase β (3.46) and (b) relative harmonic amplitude $a_2/(a_1^2 k)$ (3.47) versus wind phase ψ_P . Results are shown for Jeffreys and Generalized Miles profiles, as indicated in the legend, with $kh = \infty$, $\varepsilon = 0.1$, and pressure magnitude constant $Pk/(\rho_w g) = 1$. The Jeffreys $\beta_J = \pi/4$ is only shown at $\psi_P = \frac{1}{2}\pi$ as that is its implied ψ_P . The green dotted line represents $\psi_P = 3\pi/4$ used in many of the other plots and supported by numerical simulations from Hara & Sullivan (2015) and Husain *et al.* (2019).

4.1. Harmonic Phase, Relative Harmonic Amplitude, and Wave Shape

The harmonic phase β quantifies the relative phase shift between the primary and first harmonic and was derived (A 52) for all pressure profiles satisfying (2.17) with magnitude $Pk/(\rho_w g) = O(1)$ to $O(\varepsilon^2)$. We now specialize these results to the three pressure profiles of interest.

The complete Jeffreys harmonic phase β_J (A 52) is depicted in figs. 3a, 4a and 5a. To develop a better understanding of its functional dependence, we can consider limiting cases. For small wave-steepnesses, $\varepsilon \ll 1$, the leading order correction (3.46) is (3.46):

$$\beta_J = \pm \tan^{-1} \left(\frac{Pk/(\rho_w g)}{\tanh^2(kh) - P^2 k^2 / (\rho_w^2 g^2)} \right) + O(\varepsilon), \quad (4.2)$$

with the \pm corresponding to the sign of $\psi_P = \pm \frac{1}{2}\pi$ in the pressure profile. If we instead consider weak pressure forcing, $O(Pk/(\rho_w g)) \ll 1$, we find

$$\beta_J = \pm \frac{Pk}{\rho_w g} \coth^2(kh) + O(\varepsilon^3). \quad (4.3)$$

The Miles profile gives

$$\beta_M = 0 + O(\varepsilon^3). \quad (4.4)$$

Indeed, the HP β (3.46) vanishes (to leading order) for any $Pk/(\rho_w g) = O(1)$ pressure

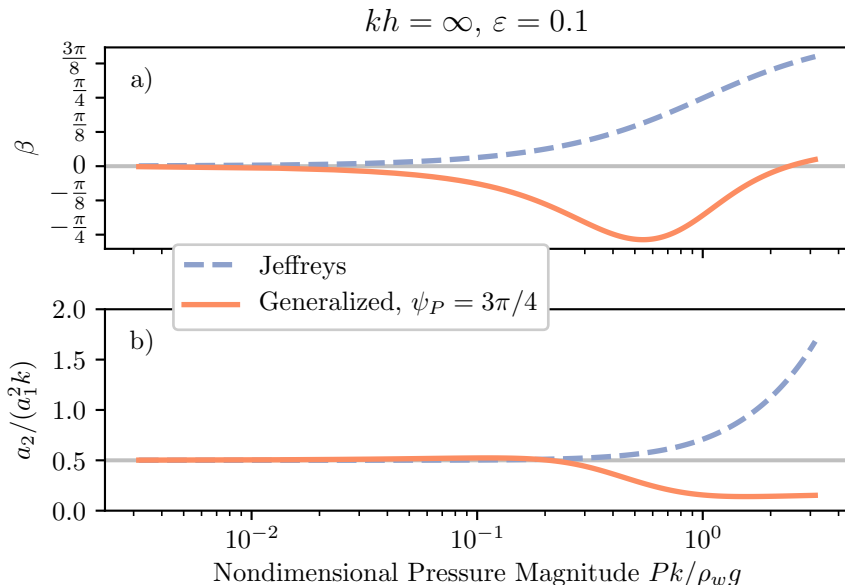


Figure 4. (Colour online) (a) Harmonic phase β (3.46) and (b) relative harmonic amplitude $a_2/(a_1^2 k)$ (3.47) versus nondimensional pressure magnitude constant $Pk/(\rho_w g)$. Results are for Jeffreys and Generalized Miles profiles, as indicated in the legend, with $kh = \infty$, $\varepsilon = 0.1$, and $\psi_P = 3\pi/4$ (for Generalized Miles).

profile of the form

$$\hat{P}_2 = \alpha + \hat{P}_1(1 + \alpha), \quad (4.5)$$

for $\alpha \in \mathbb{R}$ (Miles is $\alpha = 0$). The complete Generalized Miles β_G (A 52) is also depicted in figs. 3a, 4a and 5a. For small $\varepsilon \ll 1$, we have the approximation

$$\begin{aligned} \beta_G = \tan^{-1} & \left(\left[2 \cos \psi_P - 1 + \frac{Pk}{\rho_w g} \right] \frac{Pk}{\rho_w g} \sin \psi_P \left[- \left(\frac{Pk}{\rho_w g} \right)^2 \cos \psi_P - 1 \right. \right. \\ & \left. \left. - \frac{Pk}{\rho_w g} (\cos 2\psi_P + \cos \psi_P) + \left(1 + 2 \frac{Pk}{\rho_w g} \cos \psi_P + \left(\frac{Pk}{\rho_w g} \right)^2 \right) (2 - \sec^2(kh)) \right]^{-1} \right) \\ & + O(\varepsilon). \end{aligned} \quad (4.6)$$

Instead considering weak forcing with $O(Pk/(\rho_w g)) \ll 1$, we find

$$\begin{aligned} \beta_G = \frac{Pk}{\rho_w g} (\sin 2\psi_P - \sin \psi_P) \coth^2(kh) + \frac{1}{2} \left(\frac{Pk}{\rho_w g} \right)^2 \coth^4(h) (\sin(4\psi_P) \\ + [\sin(2\psi_P) - \sin(3\psi_P)](2 \tanh^2(h) + 1)) + O(\varepsilon^3). \end{aligned} \quad (4.7)$$

Next, we consider the relative harmonic amplitude, $a_2/(a_1^2 k)$. The complete Jeffreys relative harmonic amplitude (A 51) is shown in figs. 3b, 4b and 5b, but we can approximate

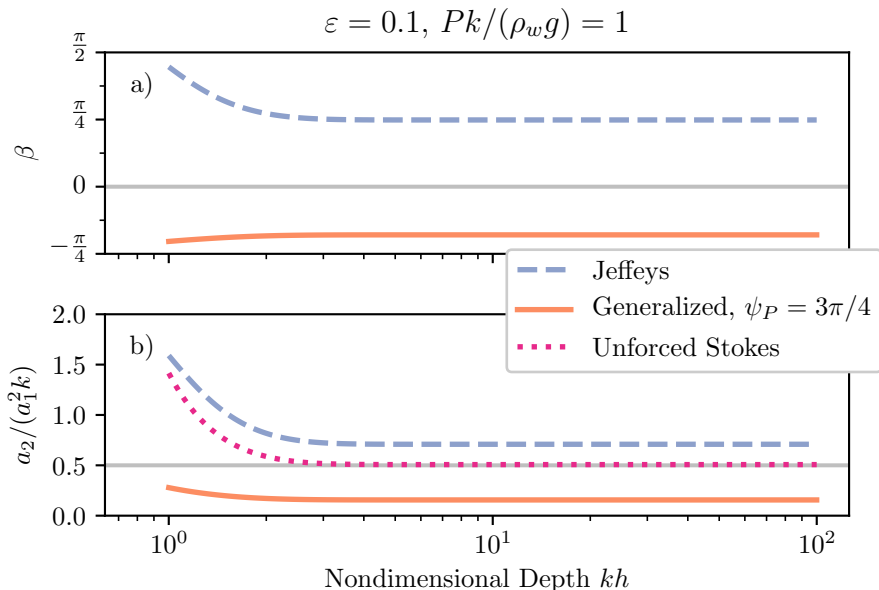


Figure 5. (Colour online) (a) Harmonic phase β (3.46) and (b) relative harmonic amplitude $a_2/(a_1^2 k)$ (3.47) versus nondimensional depth kh . Results are shown for Jeffreys and Generalized Miles profiles, as well as unforced (*i.e.* no wind) Stokes waves, with $\varepsilon = 0.1$, pressure magnitude constant $Pk/(\rho_w g) = 1$, and $\psi_P = 3\pi/4$ (for Generalized Miles).

it for small $\varepsilon \ll 1$ as (3.47)

$$\left(\frac{a_2}{a_1^2 k}\right)_J = \frac{2 + 3 \operatorname{csch}^2(kh)}{4} \coth(kh) \left\{ 1 + \left[\frac{P^2 k^2 / (\rho_w^2 g^2)}{1 + P^2 k^2 / (\rho_w^2 g^2)} \right] \times \coth^2(kh) [2 + \coth^2(kh)] \right\}^{-1} + O(\varepsilon^2). \quad (4.8)$$

However, weak wind $O(Pk/(\rho_w g)) \ll 1$ moves the P -dependence to a higher-order than we calculated, simply reverting to the unforced Stokes wave value

$$\left(\frac{a_2}{a_1^2 k}\right)_J = \frac{2 + 3 \operatorname{csch}^2(kh)}{4} \coth(kh) \left(1 + \mathcal{A}(a_1 k)^2\right) + O(\varepsilon^3), \quad (4.9)$$

with \mathcal{A} defined in (A 19). Here, the pressure forcing only plays an indirect role by causing a_1 to grow, with direct influence pushed to higher order corrections. In contrast, the Miles profile lacks a direct pressure influence even when $Pk/(\rho_w g) = O(1)$, again reducing to the unforced Stokes wave value:

$$\left(\frac{a_2}{a_1^2 k}\right)_M = \frac{2 + 3 \operatorname{csch}^2(kh)}{4} \coth(kh) \left(1 + \mathcal{A}(a_1 k)^2\right) + O(\varepsilon^3), \quad (4.10)$$

In general, the relative harmonic amplitude (3.47) $a_2/(a_1^2 k)$ reduces (to leading order in ε for $Pk/(\rho_w g) = O(1)$) to the unforced Stokes case ($\hat{P}_1 = \hat{P}_2 = 0$) precisely when

$(\hat{P}_2 - \hat{P}_1)/(1 + \hat{P}_1) = 0$, which is only satisfied by the Miles profile $\hat{P}_1 = \hat{P}_2$. Thus, the Miles profile is the unique $Pk/(\rho_w g) = O(1)$ profile type which has no impact on wave shape (β or $a_2/(a_1^2 k)$), at least to leading order in ε . The complete Generalized Miles $a_2/(a_1^2 k)_G$ (A 51) is also plotted in figs. 3b, 4b and 5b. We can simplify $a_2/(a_1^2 k)_G$ by assuming a small wave-steepness $\varepsilon \ll 1$:

$$\left(\frac{a_2}{a_1^2 k}\right)_G = \frac{2 + 3 \operatorname{csch}^2(kh)}{4} \coth(kh) \left| 1 - \coth^2(kh) \frac{(\exp\{i\psi_P\} - 1)Pk/(\rho_w g)}{1 + Pk \exp(i\psi_P)/(\rho_w g)} \right|^{-1} + O(\varepsilon). \quad (4.11)$$

Instead assuming $O(Pk/(\rho_w g)) \ll 1$ gives instead

$$\begin{aligned} \left(\frac{a_2}{a_1^2 k}\right)_G &= \frac{2 + 3 \operatorname{csch}^2(kh)}{4} \coth(kh) \left(1 + \frac{Pk}{\rho_w g} \sin \psi_P (2 \cosh \psi_P - 1) \right. \\ &\quad \left. - \frac{1}{2} \left(\frac{Pk}{\rho_w g}\right)^2 (\cos(\psi_P) - 1) \left\{ [1 + 3 \operatorname{csch}^2(kh)] \cos(\psi_P) \right. \right. \\ &\quad \left. \left. - 3 - \operatorname{csch}^2(kh) \right\} \coth^2(kh) + \mathcal{A}(a_1 k)^2 \right) + O(\varepsilon^3). \end{aligned} \quad (4.12)$$

For the chosen values of $kh = \infty$, $\varepsilon = 0.1$, and $Pk/(\rho_w g) = 1$, both the Jeffreys and Generalized Miles profiles induce a harmonic phase magnitude $|\beta|$ up to $\pi/4$ (fig. 3a). The Jeffreys value of $\beta_J = \pi/4$ is placed at $\psi_P = \frac{1}{2}\pi$ to correspond with its restriction that $\psi_P = \pm \frac{1}{2}\pi$. The Generalized Miles HP β increases from zero at $\psi_P = 0$ (fig. 3a) to roughly $\pi/16$ before decreasing to approximately $-\pi/4$ and passing through zero near $\psi_P = \frac{1}{2}\pi$ (fig. 3b). The angle $\psi_P = 3\pi/4$ is denoted by a dashed line in fig. 3, and this ψ_P is utilized hereafter, as suggested by Hara & Sullivan (2015) and Husain *et al.* (2019). In contrast to the harmonic phase, the relative harmonic amplitude shows opposing behaviour for the two forcing types. The Jeffreys $a_2/(a_1^2 k)_J = 0.7$ is enhanced relative to the deep-water Stokes value $a_2/(a_1^2 k) = \frac{1}{2}$, while the Generalized Miles value is suppressed $a_2/(a_1^2 k)_G \leq \frac{1}{2}$. Note that fig. 3 only depicts $\psi_P \geq 0$ since β (3.46) is antisymmetric and $a_2/(a_1^2 k)$ (3.47) is symmetric about $\psi_P = 0$. This is seen by noticing $\psi_P \rightarrow -\psi_P \implies \hat{P}_m \rightarrow \hat{P}_m^*$.

The wave shape parameters show a particularly rich dependence on the pressure magnitude $Pk/(\rho_w g)$ (fig. 4). While both Jeffreys and Generalized Miles yield non-zero harmonic phase β for small pressures (fig. 4a), they have qualitatively different behaviours for large $Pk/(\rho_w g)$. The Jeffreys profile increase steadily, reaching $3\pi/8$ for $Pk/(\rho_w g) = 3$. Instead, the Generalized Miles profile first decreases, reaching a minimum of approximately $-\frac{1}{4}\pi$ at $Pk/(\rho_w g) = 0.6$ and then increasing to small, positive values. The relative harmonic amplitude shows (fig. 4b) virtually no change from the deep-water Stokes value of $\frac{1}{2}$ until $Pk/(\rho_w g) = 0.3$. Then, the Jeffreys profile increases rapidly, attaining $a_2/(a_1^2 k)_J = 1.7$ for $Pk/(\rho_w g) = 3$. Contrarily, the Generalized Miles profile decreases and asymptotes to $a_2/(a_1^2 k)_G \approx 0.2$.

Finally, the nondimensional depth kh also modulates the wind effect on wave shape. For the chosen values of $Pk/(\rho_w g) = 1$ and $\psi_P = 3\pi/4$, the Generalized Miles $\beta_G \approx -\frac{1}{4}\pi$ while Jeffreys $\beta_J \approx +\frac{1}{4}\pi$ for large kh (fig. 5a). However, as the kh decreases, both values grow in magnitude with β_J increasing faster, nearly reaching $\beta_J = \frac{1}{2}\pi$ at $kh = 1$. Thus, the shallow depth kh strongly enhances the effect of wind on β . The wind's influence on $a_2/(a_1^2 k)$ is less pronounced. Notice that the unforced Stokes wave also has a depth dependence for $a_2/(a_1^2 k)$ (dashed line in fig. 5b). Though the relative harmonic amplitude is enhanced for small kh in all three cases (Jeffreys, Generalized, and unforced Stokes), notice that both pressure profiles grow slower than the unforced Stokes wave. That is, the

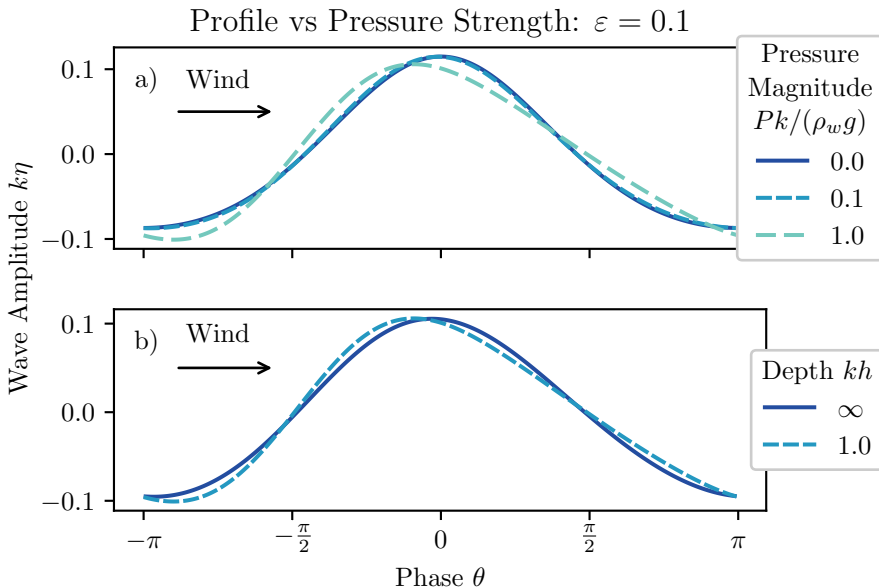


Figure 6. (Colour online) Wave profile $k\eta$ versus phase θ for $\varepsilon = 0.1$ and the Jeffreys pressure profile for (a) $kh = 1.0$ and variable $Pk/(\rho_w g)$ (see legend) and (b) $Pk/(\rho_w g) = 1.0$ and variable kh (see legend). Note that the Jeffreys profile has implied $\psi_P = +\frac{1}{2}\pi$.

pressure forcing appears to counteract shoaling-induced $a_2/(a_1^2 k)$ enhancement to some extent. Figure 5b also highlights the importance of restricting $kh \geq 1$. As kh decreases, a_2 becomes large compared to a_1 and the perturbation expansion could become disordered.

Both the harmonic phase and the relative harmonic amplitude determine the wave shape. We consider their combined influence by plotting the surface profile under the action of the Jeffreys pressure profile. Figure 6a shows how the surface profile η versus phase θ varies with $Pk/(\rho_w g) = 0, 0.1,$ and 1.0 for wind blowing to the right. The $Pk/(\rho_w g) = 0$ profile has skewness (A 56) $S = 0.3$ and asymmetry (A 57) $A = 0$ as expected for a $kh = 1$ Stokes wave. The $Pk/(\rho_w g) = 0.1$ deviates only slightly from the unforced profile. However, the $Pk/(\rho_w g) = 1$ profile shows a noticeable horizontal asymmetry, with both skewness $S = 0.05$ and asymmetry $A = 0.3$ that are fundamentally different from a Stokes wave. This follows from fig. 4a: $Pk/(\rho_w g) = 0.1$ generates a very small β_J , while β_J is significantly larger for $Pk/(\rho_w g) = 1$. We can also see that increasing depth kh decreases the influence of wind on asymmetry (fig. 6b). The $kh = \infty$ profile ($S = A = 0.1$) is less asymmetric than the $kh = 1$ profile, in agreement with fig. 5. Note that both panels of fig. 6 show the wave tilted towards the wind direction, a result of the positive β_J for Jeffreys type forcing (fig. 3a).

4.2. Phase Speed and Growth Rate

In addition to influencing wave shape, the pressure forcing terms also affect the phase speed, as predicted by Jeffreys (1925) and Miles (1957). We normalize the phase speed $c = \text{Re}\{\omega\}/k$ by the unforced, linear phase speed $c_0 = \sqrt{g \tanh(kh)}/k$. The complete fractional phase speed change $\Delta c/c_0$ is given in (A 61). If we consider small waves $\varepsilon \ll 1$,

then (A 61) simplifies considerably:

$$\begin{aligned} \frac{\Delta c}{c_0} &= \frac{|c| - |c|_{P=0}}{c_0} \\ &= \frac{1}{\sqrt{2}} \sqrt{1 + \frac{Pk}{\rho_w g} \cos \psi_P + \sqrt{1 + \left(\frac{Pk}{\rho_w g}\right)^2 + 2\frac{Pk}{\rho_w g} \cos \psi_P} - 1 + O(\varepsilon^2)}, \end{aligned} \quad (4.13)$$

with $\psi_P = \pm \frac{1}{2}\pi$ for the Jeffreys profile. If we instead assume the forcing is weak, $O(Pk/(\rho_w g)) \ll 1$, we find

$$\frac{\Delta c}{c_0} = \frac{1}{2} \frac{Pk}{\rho_w g} \cos \psi_P - \frac{1}{8} \left(\frac{Pk}{\rho_w g}\right)^2 \cos 2\psi_P + \left(a_1^2 - a_1^2 \Big|_{P=0}\right) O(\varepsilon^3), \quad (4.14)$$

For these limiting cases, we find that all three surface pressure profiles generate the same change to the phase speed; this is unsurprising since, at leading order, all three pressure profiles are equivalent (if $\psi_P = \pm \frac{1}{2}\pi$). The a_1^2 term is the amplitude-dispersion due to nonlinearity described by Stokes (1880).

As shown in section 3, the different harmonics grow at different rates; here, we will discuss the growth rate of the primary wave. It is conventional to describe the energy growth rate, $\gamma := \partial_t E/E$, rather than the amplitude growth rate, $\partial_t \eta/\eta = \text{Im}\{\omega\}$. However, since $E \propto \eta^2$, they are related as $\gamma = 2 \text{Im}\{\omega\}$. The complete nondimensional growth rate γ/f_0 is given in (A 62). For small-steepness waves, $\varepsilon \ll 1$, (A 62) simplifies to

$$\begin{aligned} \frac{\gamma}{f_0} &= \frac{4\pi \text{Im}\{\omega\}}{c_0 k} = 4\pi \text{sgn} \left(\frac{Pk}{\rho_w g} \sin \psi_P \right) \\ &\times \sqrt{-1 - P \cos \psi_P k/(\rho_w g) + \sqrt{1 + P^2 k^2/(\rho_w^2 g^2) + 2P \cos \psi_P k/(\rho_w g)}} + O(\varepsilon^2), \end{aligned} \quad (4.15)$$

with $f_0 = \text{Re}\{\omega_0\}/(2\pi) = c_0 k/(2\pi)$ the unforced, linear wave frequency. Alternatively, for weak wind forcing $O(Pk/(\rho_w g)) \ll 1$, we instead find

$$\frac{\gamma}{f_0} = 2\pi \frac{Pk}{\rho_w g} \sin \psi_P - \frac{\pi}{2} \left(\frac{Pk}{\rho_w g}\right)^2 \sin 2\psi_P + O(\varepsilon^3). \quad (4.16)$$

Both Jeffreys (1925)—with $\psi_P = \frac{1}{2}\pi$ —and Miles (1957) calculated the growth rate to leading order for weak pressure forcing $Pk/(\rho_w g) = O(\varepsilon)$; (4.16) matches their results. Naturally, if $P \rightarrow 0$, we find $\gamma \rightarrow 0$, as there is no growth.

Notice that, for both the Jeffreys and Generalized Miles profiles, the HP β and growth rate are related for small waves ($\varepsilon \ll 1$) and weak wind ($O(Pk/(\rho_w g)) \ll 1$) as

$$\begin{aligned} \begin{pmatrix} \beta_{0,M} \\ \beta_{0,G} \end{pmatrix} &= \frac{Pk}{\rho_w g} \begin{pmatrix} \pm 1 \\ \sin 2\psi_P - \sin \psi_P \end{pmatrix} \coth^2(kh) + O\left(\varepsilon \frac{Pk}{\rho_w g}\right) \\ &= \frac{1}{2\pi} \frac{\gamma}{f_0} \begin{pmatrix} 1 \\ (2 \cos \psi_P - 1) \end{pmatrix} \coth^2(kh) + O\left(\varepsilon \frac{Pk}{\rho_w g}\right). \end{aligned} \quad (4.17)$$

The connection with wave asymmetry (related to β) suggests a deeper link between wave growth and wave shape. This is potentially analogous to shoaling, weakly nonlinear waves that both grow and becomes asymmetric.

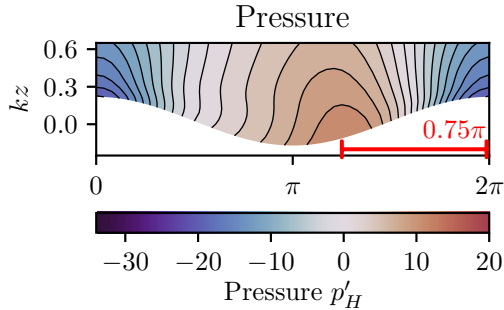


Figure 7. (Colour online) LES modelled nondimensional, perturbation air pressure over a right-propagating linear surface gravity wave as a function of nondimensional phase (kx) and kz . This simulation has nondimensional surface roughness $kz_0 = 1.35 \times 10^{-3}$, wave steepness $\varepsilon = 0.2$, and inverse wave age $u_*/c_0^\infty = 0.71$. The red line denotes the wind angle ψ_P , as measured from the wave crest to the high pressure location. Reproduced from (fig. 2, panel 2b of Husain *et al.* 2019).

5. Discussion

We have shown that the wind, via a surface pressure profile expressed as a time-independent η convolution, affects wave shape, in addition to the previously known changes in phase speed and growth rate. The different surface profiles (Jeffreys, Miles, and Generalized Miles) produce qualitatively different results. The Miles profile has no effect on wave shape, and the Generalized Miles (for $\psi_P = 3\pi/4$) HP has the opposite sign as the Jeffreys HP. Here, we will use results from large eddy simulations (section 5.1) to provide guidance on the choice of ψ_P and $Pk/(\rho_w g)$, allowing comparison with a laboratory experiment (section 5.2). We then discuss the surface pressure profiles in the context of laboratory observations and LES as well as potential future directions (section 5.3).

5.1. Using LES to Constrain the Surface Pressure

LES simulations of the airflow over a single, static, sinusoidal (*i.e.* no harmonics), deep-water wave by Husain *et al.* (2019) (see also Hara & Sullivan 2015) allow estimation of the two unknown parameters: pressure magnitude $Pk/(\rho_w g)$ and wind phase ψ_P . The Husain *et al.* (2019) simulations were based on the laboratory experiments of Buckley & Veron (2016) and explored a variety of surface roughnesses kz_0 , wave steepnesses ε , and wind speeds u_*/c_0^∞ . We consider the simulation (Husain *et al.* 2019) with intermediate surface roughness $kz_0 = 1.35 \times 10^{-3}$, appreciable wave slope $\varepsilon = 0.2$, and young waves $u_*/c_0^\infty = 0.71$ (fig. 7). The nondimensional surface perturbation pressure p'_H varies over a range from ± 20 with maximum shifted $\approx 3\pi/4$ windward of the wave crest (red bar in fig. 7), yielding our choice of $\psi_P \approx 3\pi/4$. The Husain *et al.* (2019) $\psi_P \approx 3\pi/4$ is also qualitatively consistent with the surface pressure and wave profile phase reported by Donelan *et al.* (2006). Husain *et al.* (2019) nondimensionalized pressure with the air density and friction velocity,

$$p'_H = \frac{p}{\rho_a u_*^2}, \quad (5.1)$$

whereas we nondimensionalized the pressure p' by ρ_w , g , and k . Thus, converting p'_H to p' we find

$$p' = \frac{pk}{\rho_w g} = \frac{p}{\rho_a u_*^2} \frac{u_*^2}{(c_0^\infty)^2} \frac{\rho_a}{\rho_w} = \frac{u_*^2}{(c_0^\infty)^2} \frac{\rho_a}{\rho_w} p'_H \approx 5.0 \times 10^{-4} p'_H. \quad (5.2)$$

With $u_*/c_0^\infty = 0.71$ (Husain *et al.* 2019) and $\rho_a/\rho_w \approx 10^{-3}$, $p' \approx 10^{-2}$ and $\|p'\|_2$ is $\approx 7 \times 10^{-3}$. Using their value of $\varepsilon = 0.2$ then gives $\|p'\|_2 k / (\rho_w g) \approx \varepsilon^3$, or $Pk / (\rho_w g) \approx \varepsilon^2$. Interestingly, the nondimensional pressure magnitude for this simulation is consistent with that inferred from the u_*/c_0^∞ versus γ/f_0 relationship (fig. 2), where we see that $u_*/c_0^\infty = 0.7 \implies \gamma/f_0 = 0.1$. Using (2.19) and $\psi_P = 3\pi/4$ gives $Pk / (\rho_w g) = \gamma / [2\pi f_0 \sin(\psi_P)] = 2 \times 10^{-2}$. That is, $Pk / (\rho_w g) \approx \varepsilon^2$. Thus, the results of Husain *et al.* (2019) have provided an estimate for ψ_P and a $Pk / (\rho_w g)$ consistent with our theoretical development. However, the appropriate specific pressure profile (Jeffreys, Miles, or Generalized Miles), remains to be determined; *cf.* section 5.3.

5.2. Comparison of Theory to Laboratory Wave Shape Observations

Here, we compare our predicted harmonic phase to the laboratory experiments in Leykin *et al.* (1995). We cannot compare to Feddersen & Veron (2005) as their $kh \leq 1.2$, and the u_*/c_0 to γ/f_0 relationship (fig. 2) needed for determining $Pk / (\rho_w g)$ is for deep water. In Leykin *et al.* (1995), laboratory wind-generated surface gravity waves with $\varepsilon \approx 0.15$ and $kh = 2.5$ had a quasi-linear relationship between the biphasic β at the peak frequency (the statistical analogue of our harmonic phase β) and the inverse wave age u_*/c_0 (fig. 8). For comparison, our pressure magnitude $Pk / (\rho_w g)$ must be converted to an inverse wave age u_*/c_0 (section 2.4), where we assume the deep-water relationship between u_*/c_0 and γ/f_0 (fig. 2) holds for $kh = 2.5$, which is parameterized (Banner & Song 2002) as (fig. 2, solid line)

$$\frac{\gamma}{f_0} = 32.5(2\pi) \frac{\rho_a}{\rho_w} \left(\frac{u_*}{c_0} \right)^2. \quad (5.3)$$

Using (2.19), we can relate γ/f_0 to $Pk / (\rho_w g)$ for deep-water to give

$$\frac{Pk}{\rho_w g} = \frac{32.5}{\sin \psi_P} \frac{\rho_a}{\rho_w} \left(\frac{u_*}{c_0} \right)^2 \quad (5.4)$$

allowing comparison between theory and laboratory observations.

Using (5.4), the measured inverse wave ages $u_*/c_0 = 0.5$ to 1.5 correspond to pressure magnitudes $Pk / (\rho_w g) = 0.01$ to 0.1 . Assuming a Generalized Miles pressure profile with $\psi_P = 3\pi/4$, the predicted and measured β are in qualitative agreement (compare red curve to symbols in fig. 8). We emphasize that the conversion between u_*/c_0 and $Pk / (\rho_w g)$ (5.4) is only approximate. If the conversion factor were a factor of 3 larger, the results would match reasonably well. We also note that the relatively high wind speeds (u_* up to 1.7 m s^{-1}) likely caused additional physical processes, such as whitcapping or microbreaking, to occur. Such dissipative processes are not considered in our theoretical treatment.

5.3. The Surface Pressure Profile

Most theoretical treatments of wind-induced wave growth utilize a linear theory with monochromatic waves (*e.g.* Miles 1957; Belcher & Hunt 1993; Young & Wolfe 2014). In this scenario, for the same ψ_P , the pressure profiles considered are identical at leading-order and one need not distinguish between, for instance, the Miles or Generalized Miles

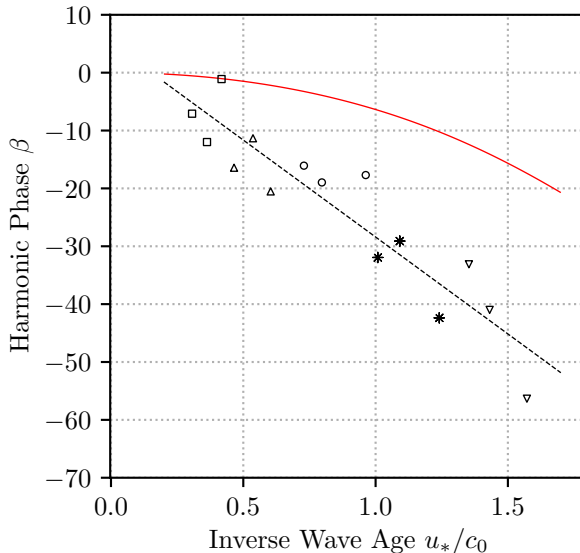


Figure 8. (Colour online) Harmonic phase β versus inverse wave age u_*/c_0 (symbols) for the Leykin *et al.* (1995) laboratory experiments. The black, dashed line is the Leykin *et al.* (1995) linear fit. Theoretical HP β (solid red) are given for the Generalized Miles pressure profile with $\psi_P = 3\pi/4$, $kh = 2.5$, and $\varepsilon = 0.15$, and conversion of u_*/c_0 to $Pk/(\rho wg)$ is given by (5.4) (*cf.* section 5.2).

profiles. However, when considering higher-order corrections to the higher harmonics, differences arise and care must be taken when choosing the pressure profile.

Direct measurements of the surface pressure profile are challenging and rare (Donelan *et al.* 2006). However, our theory can offer insight by comparing the profiles' differing effects on wave shape parameters to simulations and measurements of wind-forced waves. We have shown that the Miles pressure profile (2.12) generates no change to wave shape, in particular HP $\beta = 0$. This disagrees with the experimental measurements that find a nonzero β (Feddersen & Veron 2005; Leykin *et al.* 1995). Thus, the Miles profile appears to be an inappropriate pressure profile. Both Feddersen & Veron (2005) and Leykin *et al.* (1995) measure a harmonic phase $\beta < 0$ for co-aligned wind and waves. However, the Jeffreys profile gives a positive β while the Generalized Miles profile with $\psi_P \approx 3\pi/4$ gives a negative β (figs. 3a and 4a). Additionally, the Jeffreys requirement of $\psi_P = \pm\frac{1}{2}\pi$ appears inconsistent with numerical simulations (Hara & Sullivan 2015; Husain *et al.* 2019). This suggests that the Generalized Miles case is the more appropriate surface pressure profile of those considered here.

Throughout the derivation, we have maintained a somewhat general surface pressure profile $p(x, t)$, namely any time-independent convolution with η (*cf.* section 2.3). However, LES atmospheric simulations over a simple sinusoidal (*i.e.* no harmonics) topography (*e.g.* Hara & Sullivan 2015; Husain *et al.* 2019) result in surface pressure profiles that are not simply sinusoidal (*i.e.* they have skewness or asymmetry, *cf.* fig. 7), counter to the assumption that $\hat{p}_m \propto \hat{\eta}_m$. Our small ε theory could be extended to allow pressures with Fourier representations $\hat{p}_m = k\hat{P}_m\hat{\eta}_m + k^2\sum_n\hat{P}_{m,n}\hat{\eta}_n\hat{\eta}_m$ which could better represent the LES simulated surface pressure of Husain *et al.* (2019). Additional surface pressure complexity is likely generated if LES atmospheric simulations used a Stokes wave bottom profile instead of a single sinusoid. Allowing the wind, via surface pressure profiles, to

affect wave shape, as done here, likely induces further changes back to the airflow and surface pressure profile. That is, the air and water phases are coupled. Although this investigation relied on prescribed surface pressures, it lays the groundwork for a weakly-nonlinear coupled theory. Future work will attempt to couple the wind and waves directly, providing insight into the surface pressure profile and the related wave shape and growth.

6. Summary

Here, we derive a theory for the wind effect on the shape of surface gravity waves. The influence of the wind on ocean waves has been studied in great detail theoretically, numerically, and observationally with a principal focus on wave growth. A few laboratory and numerical experiments have shown that wind can influence wave shape, though no theory for it exists. Two key weakly-nonlinear wave shape parameters are the harmonic phase β , encoding the relative phase between the primary and harmonic (zero for unforced Stokes waves), and the relative harmonic amplitude $a_2/(a_1^2k)$. These two parameters can also be converted to the more conventional skewness and asymmetry. Motivated by prior wind-wave generation theories, three surface pressure profiles (Jeffreys, Miles, and Generalized Miles) based on a convolution with the wave profile η are prescribed. A multiple scales perturbation analysis is performed for the small wave steepness $\varepsilon := a_1k$. The deep to intermediate water theoretical solutions are derived for quasi-periodic progressive waves yielding the wind-induced changes to β and $a_2/(a_1^2k)$, as well as higher-order corrections to the previously known growth and phase speed changes. These parameters are functions of the four nondimensional parameters: the wave steepness a_1k , the depth kh , the pressure magnitude $Pk/(\rho_w g)$, and the wind angle ψ_P . By formal replacement of the pressure magnitude P with $P \rightarrow \varepsilon P$ or $P \rightarrow \varepsilon^2 P$, our derivation permits a variety of pressure magnitudes (*i.e.* wind speeds).

The Miles profile had no effect on wave shape in contrast to laboratory observations. The relative harmonic ratio $a_2/(a_1^2k)$ displayed a strong dependence on the forcing type, enhanced for Jeffreys but suppressed for Generalized Miles. The harmonic phase β had more complicated behaviour, including a local minimum for the Generalized Miles case as a function of the pressure magnitude. Despite restricting our analysis to intermediate and deep water, we found decreasing kh enhances the wind effect on wave shape. This suggests pressure forcing could play a larger role in wave shape for shallow water waves. We also found direct relationships between growth rates and β for the pressure profiles considered. Atmospheric large eddy simulations constrained both the pressure magnitude P and wind angle ψ_P . Using the constrained ψ_P , our HP predictions were qualitatively consistent with laboratory observations. Only the Generalized Miles profile could reproduce the observed sign for β , suggesting that Generalized Miles surface pressure profiles best represent the actual wave surface pressure profile. Future studies will investigate the shallow water limit. Other avenues for future work include dynamically coupling the air to the wave field. Such an approach would obviate the need to impose a specified pressure profile, increasing the applicability of the theory.

We are grateful to W. R. Young, N. Pizzo, and A. B. Villas Bôas for discussions on this work. The computations in this paper were performed by using MAPLETM (a division of Waterloo Maple Inc. 2018). We thank the National Science Foundation (OCE-1558695) and the Mark Walk Wolfinger Surfzone Processes Research Fund for their support of this work. Declaration of Interests. None.

Appendix A. Strong Forcing: $Pk/(\rho_w g) = O(1)$ ContinuedA.1. $O(\varepsilon^3)$ Equations

In section 3, we derived the leading order contributions to the HP β and relative amplitude $a_2/(a_1^2 k)$. Now, we will extend this derivation to the next non-zero correction. This will reveal a weak amplitude- and time-dependence to these shape parameters. Furthermore, by finding β and $a_2/(a_1^2 k)$ accurate to $O(\varepsilon^2)$, we can formally take $P \rightarrow \varepsilon P$ yielding solutions with $Pk/(\rho_w g) = O(\varepsilon)$, or $P \rightarrow \varepsilon^2$ generating $Pk/(\rho_w g) = O(\varepsilon^2)$ results (appendix A.5). However, the expressions begin to become unwieldy; therefore, we will only sketch the derivation. The third-order equations give

$$\frac{\partial \phi_3}{\partial z} - \frac{\partial \eta_3}{\partial t_0} = \frac{1}{2} \frac{\partial A_1}{\partial t_2} e^{i(x-\omega_0 t_0)} + A_1 |A_1|^2 \text{KIN}_{3,1} e^{i(x-\omega_0 t_0)} |e^{-i\omega_0 t_0}|^2 + A_1^3 \text{KIN}_{3,3} e^{3i(x-\omega_0 t_0)} + \text{c.c.}, \quad (\text{A } 1)$$

$$\frac{\partial \phi_3}{\partial t_0} + \eta_3 + p_3 = i \frac{1}{2} \omega_0 \frac{\partial A_1}{\partial t_2} e^{i(x-\omega_0 t_0)} \coth(h) + A_1 |A_1|^2 \text{DYN}_{3,1} e^{i(x-\omega_0 t_0)} |e^{-i\omega_0 t_0}|^2 + A_1^3 \text{DYN}_{3,3} e^{3i(x-\omega_0 t_0)} + \text{c.c.}, \quad (\text{A } 2)$$

with c.c. denoting the complex conjugate. Here, $\text{KIN}_{3,1}, \text{KIN}_{3,3}, \text{DYN}_{3,1}, \text{DYN}_{3,3} \in \mathbb{C}$ are constants that do not depend on A_1, x, t_n , or z (these dependencies have been explicitly factored out) and are composed entirely of known quantities from previous orders. In general, $\text{KIN}_{n,m}$ and $\text{DYN}_{n,m}$ are the constants (depending on h, ψ_P , and \hat{P}_m only) for the n -th order, m -th Fourier component (*i.e.*, $\exp(imkx)$) term from the kinematic or dynamic boundary condition, respectively.

Once again, inserting our Fourier transforms (3.3) to (3.5), we find

$m = 1$ Fourier Component:

$$\hat{\phi}_{3,1} - \frac{\partial \hat{\eta}_{3,1}}{\partial t_0} = \frac{\partial A_1}{\partial t_2} e^{-i\omega_0 t_0} + 2A_1 |A_1|^2 \text{KIN}_{3,1} e^{-i\omega_0 t_0} |e^{i\omega_0 t_0}|^2, \quad (\text{A } 3)$$

$$\coth(h) \frac{\partial \hat{\phi}_{3,1}}{\partial t_0} + (1 + \hat{P}_1) \hat{\eta}_{3,1} = i\omega_0 \frac{\partial A_1}{\partial t_2} e^{-i\omega_0 t_0} \coth(h) + 2A_1 |A_1|^2 \text{DYN}_{3,1} e^{-i\omega_0 t_0} |e^{-i\omega_0 t_0}|^2. \quad (\text{A } 4)$$

$m = 3$ Fourier Component:

$$3\hat{\phi}_{3,3} - \frac{\partial \hat{\eta}_{3,3}}{\partial t_0} = 2A_1^3 \text{KIN}_{3,3} e^{-3i\omega_0 t_0}, \quad (\text{A } 5)$$

$$\coth(3h) \frac{\partial \hat{\phi}_{3,3}}{\partial t_0} + (1 + \hat{P}_3) \hat{\eta}_{3,3} = 2A_1^3 \text{DYN}_{3,3} e^{-3i\omega_0 t_0}. \quad (\text{A } 6)$$

Eliminating $\hat{\phi}_{3,m}$ gives

$m = 1$ Fourier Component:

$$\coth(h) \frac{\partial^2 \hat{\eta}_{3,1}}{\partial t_0^2} + (1 + \hat{P}_1) \hat{\eta}_{3,1} = - \left(-i\omega_0 + \frac{\partial}{\partial t_0} \right) \frac{\partial A_1}{\partial t_2} e^{-i\omega_0 t_0} \coth(h) + 2A_1 |A_1|^2 [(i\omega_0 - 2 \text{Im}\{\omega_0\}) \coth(h) \text{KIN}_{3,1} + \text{DYN}_{3,1}] e^{-i\omega_0 t_0} |e^{-i\omega_0 t_0}|^2. \quad (\text{A } 7)$$

$m = 3$ Fourier Component:

$$\coth(3h) \frac{\partial^2 \hat{\eta}_{3,3}}{\partial t_0^2} + 3(1 + \hat{P}_3) \hat{\eta}_{3,3} = 6A_1^3 [i\omega_0 \coth(3h) \text{KIN}_{3,3} + \text{DYN}_{3,3}] e^{-3i\omega_0 t_0}. \quad (\text{A } 8)$$

Notice that we did not evaluate the $\partial/\partial t_0$ derivative the $(\partial/\partial t_0 - i\omega_0)$ of (A 7); we will discuss this momentarily.

Preventing secular terms requires that coefficients of $\exp(-i\omega_0 t_0)$ for $m = 1$ vanish. Thus, we require

$$\begin{aligned} \coth(h) \left(-i\omega_0 + \frac{\partial}{\partial t_0} \right) \frac{\partial A_1}{\partial t_2} e^{-i\omega_0 t_0} \\ = 2A_1 |A_1|^2 e^{-i\omega_0 t_0} e^{2 \text{Im}\{\omega_0\} t_0} [(i\omega_0 - 2 \text{Im}\{\omega_0\}) \coth(h) \text{KIN}_{3,1} + \text{DYN}_{3,1}]. \end{aligned} \quad (\text{A } 9)$$

Here, we encounter an issue: given that $A_1(t_2, t_3, \dots)$ is explicitly not a function of t_0 , there is no (nontrivial) way to satisfy the t_0 dependence of this compatibility condition. This could be dealt with rigorously by allowing the fast timescale t_0 to modulate the slower timescales when we defined our multiple scales expansion.

We encounter this issue because the growth on the fast timescale affects the period of the slower timescales. This could be dealt with formally if we had instead defined our multiple scale expansion with additional, fast-timescale dependences:

$$\frac{dt'_0}{dt} = 1, \quad \frac{d}{dt'_1} = \varepsilon \mu_1(t'_0), \quad \frac{dt'_2}{dt} = \varepsilon^2 \mu_2(t'_0), \quad \dots, \quad \frac{dt'_n}{dt} = \varepsilon^n \mu_n(t'_0), \quad (\text{A } 10)$$

with the primes to make our new timescales distinct from the originally defined ones. Then, we can choose the form of μ_n to remove secular terms. This modified multiple scales approach is similar to the one specified in Pedersen (2006).

Using this freedom to remove these problematic secularities, we would find that

$$\mu_n(t'_0) = e^{n \text{Im}\{\omega_0\} t'_0}. \quad (\text{A } 11)$$

This method would eliminate the need to be careful about the $(\partial/\partial t'_0 - i\omega_0) \partial A_1/\partial t'_2$ term previously mentioned, and would eliminate the $e^{2 \text{Im}\{\omega_0\} t'_0}$ term we are attempting to deal with currently. Later, to re-express the solution in terms of t , a simple integration yields

$$t'_n = \frac{\varepsilon^n}{n \text{Im}\{\omega_0\}} \left(e^{n \text{Im}\{\omega_0\} t} - 1 \right). \quad (\text{A } 12)$$

where we required that $t'_n = 0$ at $t = 0$. Note: t'_0 is not a special case; treating n as a continuous variable and taking the limit $n \rightarrow 0$ recovers $t'_0 = t$.

Note that, since our previous solutions had no t_1 dependence, making this *post hoc* change to t_2 does not alter any of our previous conclusions. Furthermore, we will see that only the even timescales ($t_2, t_4, \text{etc.}$) need this treatment; since we are only considering timescales up to t_3 , we will only make this replacement for t_2 .

Making this redefinition, our compatibility conditions becomes

$$\begin{aligned} \coth(h) \left(-i\omega_0 + \frac{\partial}{\partial t_0} \right) \frac{\partial A_1}{\partial t'_2} e^{-i\omega_0 t_0} e^{2 \text{Im}\{\omega_0\} t_0} = \\ 2A_1 |A_1|^2 e^{-i\omega_0 t_0} e^{2 \text{Im}\{\omega_0\} t_0} [(i\omega_0 - 2 \text{Im}\{\omega_0\}) \coth(h) \text{KIN}_{3,1} + \text{DYN}_{3,1}], \end{aligned} \quad (\text{A } 13)$$

which simplifies to

$$\begin{aligned} \coth(h) \frac{\partial A_1}{\partial t'_2} &= A_1 |A_1|^2 \frac{(i\omega_0 - 2 \operatorname{Im}\{\omega_0\}) \coth(h) \operatorname{KIN}_{3,1} + \operatorname{DYN}_{3,1}}{-i\omega_0 + \operatorname{Im}\{\omega_0\}} \\ &:= -iA_1 |A_1|^2 \operatorname{COMB}_{3,1}, \end{aligned} \quad (\text{A } 14)$$

where we defined

$$\operatorname{COMB}_{3,1} := i \frac{(i\omega_0 - 2 \operatorname{Im}\{\omega_0\}) \coth(h) \operatorname{KIN}_{3,1} + \operatorname{DYN}_{3,1}}{-i\omega_0 + \operatorname{Im}\{\omega_0\}}. \quad (\text{A } 15)$$

Now, if we assume a solution of the form

$$A_1(t'_2) = \rho(t'_2) e^{i\psi(t'_2)},$$

with $\rho(t'_2), \psi(t'_2) \in \mathbb{R}$, yields

$$\frac{\partial \rho}{\partial t'_2} + i\rho \frac{\partial \psi}{\partial t'_2} = -i\rho^3 \operatorname{COMB}_{3,1}. \quad (\text{A } 16)$$

Collecting real and imaginary parts and solving yields

$$\begin{aligned} A_1(t'_2) &= A'_1 \exp \left[i \frac{1}{2} \ln \left(1 - 2|A'_1|^2 t'_2 \operatorname{Im}\{\operatorname{COMB}_{3,1}\} \right) \frac{\operatorname{Re}\{\operatorname{COMB}_{3,1}\}}{\operatorname{Im}\{\operatorname{COMB}_{3,1}\}} \right] \\ &\quad \div \sqrt{1 - 2|A'_1|^2 t'_2 \operatorname{Im}\{\operatorname{COMB}_{3,1}\}}, \end{aligned} \quad (\text{A } 17)$$

with $A'_1(t_3) \in \mathbb{C}$. Later, converting back to t will give

$$\begin{aligned} A_1(t) &= A'_1 \exp \left\{ \frac{i}{2} \ln \left[1 - \varepsilon^2 |A'_1|^2 \left(e^{2 \operatorname{Im}\{\omega_0\} t} - 1 \right) \frac{\operatorname{Im}\{\operatorname{COMB}_{3,1}\}}{\operatorname{Im}\{\omega_0\}} \right] \frac{\operatorname{Re}\{\operatorname{COMB}_{3,1}\}}{\operatorname{Im}\{\operatorname{COMB}_{3,1}\}} \right\} \\ &\quad \div \sqrt{1 - \varepsilon^2 |A'_1|^2 \left(e^{2 \operatorname{Im}\{\omega_0\} t} - 1 \right) \frac{\operatorname{Im}\{\operatorname{COMB}_{3,1}\}}{\operatorname{Im}\{\omega_0\}}}. \end{aligned} \quad (\text{A } 18)$$

Note that, if $p \rightarrow 0$, then $\operatorname{COMB}_{3,1}$ reduces to the real quantity

$$\begin{aligned} \operatorname{COMB}_{3,1} \Big| &:= \mathcal{A} = \frac{1}{384[2 + 3 \operatorname{csch}^2(h)]} (272 + 856 \operatorname{csch}^2(h) + 512 \operatorname{csch}^4(h) \\ &\quad - 558 \operatorname{csch}^6(h) - 567 \operatorname{csch}^8(h) - 81 \operatorname{csch}^{10}(h)). \end{aligned} \quad (\text{A } 19)$$

With the compatibility condition solved, the $m = 1$ equation reduces to the homogeneous equation; for simplicity, we will choose

$$\hat{\eta}_{3,1} = 0.$$

Substituting (A 14) and our solution for $\hat{\eta}_{3,1}$ into the surface boundary conditions allows us to solve for $\hat{\phi}_{3,1}$. Assuming a solution of the form

$$\hat{\phi}_{3,1} = C_{3,1} A_1 |A_1|^2 e^{-i\omega_0 t_0} e^{2 \operatorname{Im}\{\omega_0\} t_0},$$

yields

$$C_{3,1} = \frac{-i\omega_0 \operatorname{KIN}_{3,1} + \tanh(h) \operatorname{DYN}_{3,1}}{-i\omega_0 + \operatorname{Im}\{\omega_0\}}. \quad (\text{A } 20)$$

The second harmonic ($m = 3$) equation is solved for $\hat{\eta}_{3,3}$ as usual. Then, substituting this solution into the surface boundary conditions permits solving for $\hat{\phi}_{3,3}$.

Thus, we have the solutions

$$\begin{aligned} \phi_3 = C_{3,1} A_1 |A_1|^2 e^{2\text{Im}\{\omega_0\}t_0} e^{i(x-\omega_0 t_0)} \frac{\cosh(z+h)}{\sinh(h)} \\ + C'_{3,3} A_1^3 e^{3i(x-\omega_0 t_0)} \frac{\cosh[3(z+h)]}{\sinh(3h)}, \end{aligned} \quad \eta_3 = C_{3,3} A_1^3 e^{3i(x-\omega_0 t_0)} \quad (\text{A } 21)$$

with

$$C_{3,1} = \frac{-i\omega_0 \text{KIN}_{3,1} + \tanh(h) \text{DYN}_{3,1}}{-i\omega_0 + \text{Im}\{\omega_0\}}, \quad (\text{A } 22)$$

$$C'_{3,3} = 2 \frac{(1 + \hat{P}_3) \text{KIN}_{3,3} - 3i\omega_0 \text{DYN}_{3,3}}{-9\omega_0^2 \coth(3h) + 3(1 + \hat{P}_3)}, \quad (\text{A } 23)$$

$$C_{3,3} = 6 \frac{(-i\omega_0 - 2\text{Im}\{\omega_0\}) \coth(h) \text{KIN}_{3,3} + \text{DYN}_{3,3}}{-9\omega_0^2 \coth(3h) + 3(1 + \hat{P}_3)}. \quad (\text{A } 24)$$

A.2. $O(\varepsilon^4)$ Equations

Finally, going to fourth-order, we have

$$\begin{aligned} \frac{\partial \phi_4}{\partial z} - \frac{\partial \eta_4}{\partial t_0} = \frac{1}{2} \frac{\partial A_1}{\partial t_3} e^{i(x-\omega_0 t_0)} \\ + \text{KIN}_{4,0} |e^{-i\omega_0 t_0}|^4 + \text{KIN}_{4,2} e^{2i(x-\omega_0 t_0)} |e^{-i\omega_0 t_0}|^2 + \text{KIN}_{4,4} e^{4i(x-\omega_0 t_0)} + \text{c.c.}, \end{aligned} \quad (\text{A } 25)$$

$$\begin{aligned} \frac{\partial \phi_4}{\partial t_0} + \eta_4 + p_4 = i \frac{1}{2} \omega_0 \frac{\partial A_1}{\partial t_3} e^{i(x-\omega_0 t_0)} \coth(h) \\ + \text{DYN}_{4,0} |e^{-i\omega_0 t_0}|^4 + \text{DYN}_{4,2} e^{2i(x-\omega_0 t_0)} |e^{-i\omega_0 t_0}|^2 + \text{DYN}_{4,4} e^{4i(x-\omega_0 t_0)} + \text{c.c.} \end{aligned} \quad (\text{A } 26)$$

Here, $\text{KIN}_{4,0}, \text{KIN}_{4,2}, \text{KIN}_{4,4}, \text{DYN}_{4,0}, \text{DYN}_{4,2}, \text{DYN}_{4,4} \in \mathbb{C}$ are constants that do not depend on A_1 , x , t_n , or z (these dependencies have been explicitly factored out) and are composed entirely of known quantities from previous orders.

Inserting the Fourier transforms (3.3) to (3.5) gives

$m = 2$ Fourier Component:

$$2\hat{\phi}_{4,2} - \frac{\partial \hat{\eta}_{4,2}}{\partial t_0} = 2A_1^2 |A_1|^2 \text{KIN}_{4,2} e^{2i(x-\omega_0 t_0)} |e^{-i\omega_0 t_0}|^2, \quad (\text{A } 27)$$

$$\frac{\partial \hat{\phi}_{4,2}}{\partial t_0} \coth(2h) + (1 + \hat{P}_2) \hat{\eta}_{4,2} = 2A_1^2 |A_1|^2 \text{DYN}_{4,2} e^{2i(x-\omega_0 t_0)} |e^{-i\omega_0 t_0}|^2, \quad (\text{A } 28)$$

$m = 4$ Fourier Component:

$$4\hat{\phi}_{4,4} - \frac{\partial \hat{\eta}_{4,4}}{\partial t_0} = 2A_1^4 \text{KIN}_{4,4} e^{4i(x-\omega_0 t_0)}, \quad (\text{A } 29)$$

$$\frac{\partial \hat{\phi}_{4,4}}{\partial t_0} \coth(4h) + (1 + \hat{P}_4) \hat{\eta}_{4,4} = 2A_1^4 \text{DYN}_{4,4} e^{4i(x-\omega_0 t_0)}, \quad (\text{A } 30)$$

$m = 0$ Fourier Component:

$$-\frac{\partial \hat{\eta}_{4,0}}{\partial t_0} = 2|A_1|^4 \text{KIN}_{4,0} |e^{-i\omega_0 t_0}|^4, \quad (\text{A 31})$$

$$\frac{\partial \hat{\phi}_{4,0}}{\partial t_0} + \hat{\eta}_{4,0} = 2|A_1|^4 \text{DYN}_{4,0} |e^{-i\omega_0 t_0}|^4, \quad (\text{A 32})$$

$m = 1$ Fourier Component:

$$\hat{\phi}_{4,1} - \frac{\partial \hat{\eta}_{4,1}}{\partial t_0} = \frac{\partial A_1}{\partial t_3} e^{-i\omega_0 t_0}, \quad (\text{A 33})$$

$$\frac{\partial \hat{\phi}_{4,1}}{\partial t_0} \coth(h) + (1 + \hat{P}_1) \hat{\eta}_{4,1} = i\omega_0 \frac{\partial A_1}{\partial t_3} e^{-i\omega_0 t_0} \coth(h), \quad (\text{A 34})$$

with asterisk representing complex conjugation.

Again, eliminating $\hat{\eta}_4$ gives

$m = 2$ Fourier Component:

$$\begin{aligned} \frac{\partial^2 \hat{\phi}_{4,2}}{\partial t_0^2} \coth(2h) + 2(1 + \hat{P}_2) \hat{\phi}_{4,2} = 2A_1^2 |A_1|^2 e^{-2i\omega_0 t_0} e^{2\text{Im}\{\omega_0\}t_0} \left[(1 + \hat{P}_2) \text{KIN}_{4,2} \right. \\ \left. + 2(-i\omega_0 + \text{Im}\{\omega_0\}) \text{DYN}_{4,2} \right]. \end{aligned} \quad (\text{A 35})$$

$m = 4$ Fourier Component:

$$\frac{\partial^2 \hat{\phi}_{4,4}}{\partial t_0^2} \coth(4h) + 4(1 + \hat{P}_4) \hat{\phi}_{4,4} = 2A_1^4 e^{-4i\omega_0 t_0} \left[(1 + \hat{P}_4) \text{KIN}_{4,4} - 4i\omega_0 \text{DYN}_{4,4} \right]. \quad (\text{A 36})$$

$m = 0$ Fourier Component:

$$\frac{\partial^2 \hat{\phi}_{4,0}}{\partial t_0^2} = 2|A_1|^4 e^{4\text{Im}\{\omega_0\}t_0} [\text{KIN}_{4,0} + 4\text{Im}\{\omega_0\} \text{DYN}_{4,0}]. \quad (\text{A 37})$$

$m = 1$ Fourier Component:

$$\frac{\partial^2 \hat{\phi}_{4,1}}{\partial t_0^2} \coth(h) + (1 + \hat{P}_1) \hat{\phi}_{4,1} = 2(1 + \hat{P}_1) \frac{\partial A_1}{\partial t_3} e^{-i\omega_0 t_0}. \quad (\text{A 38})$$

Preventing secular terms requires that $\partial_{t_3} A_1 = 0$. These can be solved as usual for $\hat{\phi}_{4,m}$; using the surface boundary conditions, the solutions for $\hat{\eta}_{4,m}$ can then be determined as well.

The only terms worth discussing are the zero-modes, $\hat{\phi}_{4,0}$ and $\hat{\eta}_{4,0}$. While $\hat{\eta}_{4,0}$ has physical meaning (this is a component of the setup or setdown), $\hat{\phi}_{4,0}$ has a gauge freedom: we may add a constant term (in x and t_0), as well as a term proportional to t_0 , without affecting any observables. Using this freedom, we will choose these two free constants such that the $\hat{\eta}_{4,0} \rightarrow 0$ and $\hat{\phi}_{4,0} \rightarrow 0$ as $P \rightarrow 0$.

The solutions at this order are

$$\begin{aligned} \phi_4 = & C'_{4,2} A_1^2 |A_1|^2 e^{2i(x-\omega_0 t_0)} e^{2\text{Im}\{\omega_0\} t_0} \frac{\cosh[2(z+h)]}{\sinh(2h)} + C'_{4,4} A_1^4 e^{4i(x-\omega_0 t_0)} \frac{\cosh[4(z+h)]}{\sinh(4h)} \\ & + C'_{4,0} \left(|A_1|^4 e^{4\text{Im}\{\omega_0\} t_0} - |\tilde{A}_1|^4 \right) + t_0 C_{4,0} |\tilde{A}_1|^4, \end{aligned} \quad (\text{A } 39)$$

$$\begin{aligned} \eta_4 = & C_{4,2} A_1^2 |A_1|^2 e^{2i(x-\omega_0 t_0)} e^{2\text{Im}\{\omega_0\} t_0} + C_{4,4} A_1^4 e^{4i(x-\omega_0 t_0)} \\ & + C_{4,0} \left(|A_1|^4 e^{4\text{Im}\{\omega_0\} t_0} - |\tilde{A}_1|^4 \right), \end{aligned} \quad (\text{A } 40)$$

with

$$C_{4,0} = -\frac{\text{KIN}_{4,0}}{2\text{Im}\{\omega_0\}}, \quad (\text{A } 41)$$

$$C_{4,2} = \frac{(i\omega_0 - \text{Im}\{\omega_0\}) \coth(2h) \text{KIN}_{4,2} + \text{DYN}_{4,2}}{2(-i\omega_0 + \text{Im}\{\omega_0\})^2 \coth(2h) + (1 + \hat{P}_2)}, \quad (\text{A } 42)$$

$$C_{4,4} = 2 \frac{i\omega_0 \coth(4h) \text{KIN}_{4,4} + \text{DYN}_{4,4}}{-4\omega_0^2 \coth(4h) + (1 + \hat{P}_4)}, \quad (\text{A } 43)$$

$$C'_{4,0} = \frac{\text{KIN}_{4,0} + 4\text{Im}\{\omega_0\} \text{DYN}_{4,0}}{8\text{Im}\{\omega_0\}^2}, \quad (\text{A } 44)$$

$$C'_{4,2} = \frac{(1 + \hat{P}_2) \text{KIN}_{4,2} + 2(-i\omega_0 + \text{Im}\{\omega_0\}) \text{DYN}_{4,2}}{2(-i\omega_0 + \text{Im}\{\omega_0\})^2 \coth(2h) + (1 + \hat{P}_2)}, \quad (\text{A } 45)$$

$$C'_{4,4} = \frac{(1 + \hat{P}_4) \text{KIN}_{4,4} - 4i\omega_0 \text{DYN}_{4,4}}{-8\omega_0^2 \coth(4h) + 2(1 + \hat{P}_4)}. \quad (\text{A } 46)$$

Here, $\tilde{A}_1 := A_1|_{P=0}$ is the additive ‘‘constant’’ we were permitted from the $m = 0$ equation; note: \tilde{A}_1 could still be a function of slower timescales $t_1, t_2, \text{etc.}$ As mentioned previously, a term, linear in t_0 , was included in $\hat{\phi}_{4,0}$; this was necessary to include the \tilde{A}_1 term in $\hat{\eta}_{4,0}$. For reference, the full solution for η is

$$\begin{aligned} \eta = & \text{Re} \left\{ \varepsilon A_1 e^{i(x-\omega_0 t_0)} + \varepsilon^2 A_1^2 C_{2,2} e^{2i(x-\omega_0 t_0)} + \varepsilon^3 A_1^3 C_{3,3} e^{3i(x-\omega_0 t_0)} \right. \\ & \left. + \varepsilon^4 \left(A_1^4 C_{4,4} e^{4i(x-\omega_0 t_0)} + A_1^2 |A_1|^2 e^{2\text{Im}\{\omega_0\} t_0} e^{2i(x-\omega_0 t_0)} \right) \right\} + O(\varepsilon^5), \end{aligned} \quad (\text{A } 47)$$

with $A_1(t_2)$ given by (A 17).

A.3. Shape Parameters

Now, we can calculate the shape parameters when pressure enters at leading order. Recall that we are seeking two parameters—the HP β , and the relative harmonic amplitude, $a_2/(a_1^2 k)$ (with a_2 the amplitude of the *complete* first harmonic, and a_1 the amplitude of the complete primary).

The primary wave is simply

$$\eta_{m=1} = \varepsilon A_1 e^{i(x-\omega_0 t_0)} + O(\varepsilon^5), \quad (\text{A } 48)$$

with $A_1(t_2)$ given by (A 17).

The first harmonic has two components; we calculated the $O(\varepsilon^2)$ contribution in (3.38), and the $O(\varepsilon^4)$ contribution in (A 40). Combining these, we have the first-harmonic

$$\eta_{m=2} = \varepsilon^2 A_1^2 e^{2i(x-\omega_0 t_0)} C_{2,2} + \varepsilon^4 A_1^2 |A_1|^2 e^{2i(x-\omega_0 t_0)} e^{2\text{Im}\{\omega_0\}t_0} C_{4,2} + O(\varepsilon^5) \quad (\text{A } 49)$$

with $C_{2,2}$ defined in (3.40) as

$$C_{2,2} := \frac{1}{4} (2 + 3 \text{csch}^2(h)) \coth(h) \frac{1 + \hat{P}_1}{1 + \hat{P}_1 - \coth^2(h) [\hat{P}_2 - \hat{P}_1]},$$

and $C_{4,2}$ defined in (A 42) as

$$C_{4,2} = \frac{(i\omega_0 - \text{Im}\{\omega_0\}) \coth(2h) \text{KIN}_{4,2} + \text{DYN}_{4,2}}{2(-i\omega_0 + \text{Im}\{\omega_0\})^2 \coth(2h) + (1 + \hat{P}_2)}.$$

See (A 68) for the full expression.

To find the relative harmonic amplitude and HP, we will need to calculate the ratio of the first harmonic, $\hat{\eta}_{m=2}$, to the primary, $\hat{\eta}_{m=1}$, squared (*cf.* (3.43) and (3.45)):

$$\frac{\hat{\eta}_{m=2}}{\hat{\eta}_{m=1}^2} = C_{2,2} + \varepsilon^2 |A_1|^2 e^{2\text{Im}\{\omega_0\}t_0} C_{4,2} + O(\varepsilon^3). \quad (\text{A } 50)$$

Now, the relative harmonic amplitude (3.43), $a_2/(a_1^2 k)$, is the magnitude of this quantity,

$$\begin{aligned} \frac{a_2}{a_1^2 k} &= \left| C_{2,2} + \varepsilon^2 |A_1|^2 e^{2\text{Im}\{\omega_0\}t_0} C_{4,2} \right| + O(\varepsilon^3) \\ &= |C_{2,2}| \left(1 + \varepsilon^2 |A_1|^2 e^{2\text{Im}\{\omega_0\}t_0} \text{Re}\{C_{4,2} C_{2,2}^*\} \right) + O(\varepsilon^3). \end{aligned} \quad (\text{A } 51)$$

We can see that the $O(\varepsilon^2)$ correction grows as a function of the fast timescale, t_0 , as well as the slow timescale, t_2' (through its $A_1(t_2)$ dependence).

Likewise, the HP β is the complex angle (3.45) of (A 50):

$$\begin{aligned} \beta &:= \tan^{-1} \left(\frac{\text{Im}\{C_{2,2} + \varepsilon^2 |A_1|^2 e^{2\text{Im}\{\omega_0\}t_0} C_{4,2}\}}{\text{Re}\{C_{2,2} + \varepsilon^2 |A_1|^2 e^{2\text{Im}\{\omega_0\}t_0} C_{4,2}\}} \right) + O(\varepsilon^3) \\ &\approx \beta_0 + \varepsilon^2 |A_1|^2 e^{2\text{Im}\{\omega_0\}t_0} \frac{\text{Re}\{C_{2,2}\} \text{Im}\{C_{2,2}\}}{\text{Re}\{C_{2,2}\}^2 + \text{Im}\{C_{2,2}\}^2} \left(\frac{\text{Im}\{C_{4,2}\}}{\text{Im}\{C_{2,2}\}} - \frac{\text{Re}\{C_{4,2}\}}{\text{Re}\{C_{2,2}\}} \right) + O(\varepsilon^3), \end{aligned} \quad (\text{A } 52)$$

with β_0 given in (3.46) by

$$\beta_0 = \tan^{-1} \left(\frac{\text{Im}\left\{ \left[\hat{P}_2 - \hat{P}_1 \right] \left(1 + \hat{P}_1^* \right) \right\}}{\left| 1 + \hat{P}_1 \right|^2 \tanh^2(h) - \text{Re}\left\{ \left[\hat{P}_2 - \hat{P}_1 \right] \left(1 + \hat{P}_1^* \right) \right\}} \right),$$

with a asterisk representing the complex conjugate. Notice that β now begins to show a weak amplitude, $|A_1|$, dependence.

Asymmetry and skewness are more common shape parameters than β and $a_2/(a_1^2 k)$. Therefore, we derive the asymmetry and skewness of our solution. The skewness S and

asymmetry A of a wave are defined as

$$S := \frac{\langle \eta^3 \rangle}{\langle \eta^2 \rangle^{3/2}}, \quad (\text{A } 53)$$

$$A := \frac{\langle \mathcal{H}\{\eta\}^3 \rangle}{\langle \eta^2 \rangle^{3/2}}, \quad (\text{A } 54)$$

with $\langle \cdot \rangle$ the spatial average over one wavelength and $\mathcal{H}\{\cdot\}$ the Hilbert transform (in x). The average of any Fourier component $\exp(imx)$ over a wavelength is zero for $m \neq 0 \in \mathbb{N}$. Therefore, only the combinations wherein the x -dependence cancels will contribute. Inserting our solution

$$\eta = \text{Re} \left\{ \varepsilon A_1 e^{i(x - \omega_0 t_0)} + \varepsilon^2 A_1^2 C_{2,2} e^{2i(x - \omega_0 t_0)} \right\} + O(\varepsilon^3), \quad (\text{A } 55)$$

yields

$$S = \frac{3}{\sqrt{2}} \varepsilon |A_1| e^{\text{Im}\{\omega_0\}t_0} \text{Re}\{C_{2,2}\} + O(\varepsilon^2), \quad (\text{A } 56)$$

$$A = \frac{3}{\sqrt{2}} \varepsilon |A_1| e^{\text{Im}\{\omega_0\}t_0} \text{Im}\{C_{2,2}\} + O(\varepsilon^2). \quad (\text{A } 57)$$

Here, we only calculated the $O(\varepsilon)$ contribution for brevity; using the full solution (A 47) for η would yield a solution accurate up to and including $O(\varepsilon^3)$ terms.

A.4. Complex Frequency

After deriving our solutions (A 48) and (A 49), it is useful to repackage them in a more conventional notation. Therefore, we will gather the entire time dependence into a complex phase $\Theta \in \mathbb{C}$, from which we can extract a complex, time-dependent frequency $\omega(t) \in \mathbb{C}$ giving both propagation and growth. From (A 18), we can write the entire t -dependence of $A_1(t)$ as a complex phase:

$$A_1(t) = A'_1 \exp \left\{ i \frac{1}{2} \frac{\text{COMB}_{3,1}}{\text{Im}\{\text{COMB}_{3,1}\}} \ln \left[1 - \varepsilon^2 |A'_1|^2 \left(e^{2\text{Im}\{\omega_0\}t} - 1 \right) \frac{\text{Im}\{\text{COMB}_{3,1}\}}{\text{Im}\{\omega_0\}} \right] \right\} + O(\varepsilon^4). \quad (\text{A } 58)$$

Therefore, the entire complex phase Θ of the first harmonic $\eta_{m=1} = A'_1 \exp(i\Theta)$ is

$$\Theta := kx - \omega_0 t_0 + i \frac{1}{2} \frac{\text{COMB}_{3,1}}{\text{Im}\{\text{COMB}_{3,1}\}} \ln \left[1 - \varepsilon^2 |A'_1|^2 \left(e^{2\text{Im}\{\omega_0\}t} - 1 \right) \frac{\text{Im}\{\text{COMB}_{3,1}\}}{\text{Im}\{\omega_0\}} \right] + O(\varepsilon^4). \quad (\text{A } 59)$$

Now, we define the full, complex frequency as

$$\omega := -\frac{\partial S}{\partial t} = \omega_0 + \varepsilon^2 |A'_1|^2 e^{2\text{Im}\{\omega_0\}t} \text{COMB}_{3,1} \left[1 - \varepsilon^2 |A'_1|^2 \left(e^{2\text{Im}\{\omega_0\}t} - 1 \right) \frac{\text{Im}\{\text{COMB}_{3,1}\}}{\text{Im}\{\omega_0\}} \right]^{-1} + O(\varepsilon^4). \quad (\text{A } 60)$$

Notice that the time-dependence of ω is a manifestation of the (time-dependent) amplitude dispersion of unforced Stokes waves. Then, the phase speed is the real part of

ω ,

$$c := \operatorname{Re}\{\omega\} = \operatorname{Re}\{\omega_0\} + \varepsilon^2 |A'_1|^2 e^{2\operatorname{Im}\{\omega_0\}t} \operatorname{Re}\{\operatorname{COMB}_{3,1}\} \left[1 - \varepsilon^2 |A'_1|^2 \left(e^{2\operatorname{Im}\{\omega_0\}t} - 1 \right) \frac{\operatorname{Im}\{\operatorname{COMB}_{3,1}\}}{\operatorname{Im}\{\omega_0\}} \right]^{-1} + O(\varepsilon^4), \quad (\text{A } 61)$$

while the growth rate is the imaginary

$$\gamma := \operatorname{Im}\{\omega\} = \operatorname{Im}\{\omega_0\} + \varepsilon^2 |A'_1|^2 e^{2\operatorname{Im}\{\omega_0\}t} \operatorname{Im}\{\operatorname{COMB}_{3,1}\} \left[1 - \varepsilon^2 |A'_1|^2 \left(e^{2\operatorname{Im}\{\omega_0\}t} - 1 \right) \frac{\operatorname{Im}\{\operatorname{COMB}_{3,1}\}}{\operatorname{Im}\{\omega_0\}} \right]^{-1} + O(\varepsilon^4). \quad (\text{A } 62)$$

It is natural to define the (dimensional) harmonic amplitudes a_n of (A 47) as containing the growth time-dependence:

$$a_1(t) := |\hat{\eta}_{m=1}| = \varepsilon \frac{|A'_1|}{k} e^{\operatorname{Im}\{\Theta\}} + O(\varepsilon^5), \quad (\text{A } 63)$$

$$a_2(t) := |\hat{\eta}_{m=2}| = \varepsilon^2 \frac{|A'_1|^2}{k} e^{2\operatorname{Im}\{\Theta\}} \left[1 + \varepsilon^2 |A_1|^2 e^{2\operatorname{Im}\{\omega_0\}t} \right] + O(\varepsilon^5) \quad (\text{A } 64)$$

$$= \varepsilon^2 \frac{|A'_1|^2}{k} e^{2\operatorname{Im}\{\Theta\}} \left[1 + (a_1 k)^2 \right] + O(\varepsilon^5), \quad (\text{A } 65)$$

where we made the approximation $\operatorname{Im}\{\omega_0\}t_0 \approx \operatorname{Im}\{\Theta\}$ in the final line. This leaves the propagation time-dependence given by the (real) phase

$$\theta := \operatorname{Re}\{\Theta\} = kx - \int \operatorname{Re}\{\omega\} dt, \quad (\text{A } 66)$$

such that the dimensional solution is

$$k\eta = (a_1 k) e^{i\theta} + (a_1 k)^2 \frac{a_2}{a_1^2 k} e^{2i\theta + \beta} + \dots \quad (\text{A } 67)$$

A.5. Weaker Wind Forcing

In appendices A.1 and A.2 we performed the derivation up to $O(\varepsilon^4)$ with a pressure forcing $Pk/(\rho_w g) = O(1)$. This yielded expressions (A 51), (A 52) and (A 60) for $a_2/(a_1^2 k)$, β , and $\omega \in \mathbb{C}$ accurate to $O(\varepsilon^3)$. However, it is occasionally useful to consider weaker winds, such as $Pk/(\rho_w g) = O(\varepsilon)$ or $O(\varepsilon^2)$, as discussed in section 2.4. These results can be generated by formally replacing $P \rightarrow \varepsilon P$ or $P \rightarrow \varepsilon^2 P$, respectively, in (A 51), (A 52) and (A 60) and dropping terms $O(\varepsilon^3)$ or higher. We have also performed the derivation by simply assuming $Pk/(\rho_w g) = O(\varepsilon^2)$ *a priori* (not included here). For the appropriate $O(Pk/(\rho_w g))$, this simpler but limited solution and the general (appendix A) solution give consistent results after converting back to the true time t . This further confirms the wide parameter range of the $Pk/(\rho_w g) = O(1)$ derivation (section 3 and appendix A).

A.6. Full $C_{4,2}$ Expression

Here, we give the full expression for $C_{4,2}$, defined in (A 42) as the coefficient of the $O(\varepsilon^4)$ correction to the $m = 2$ harmonic of η .

$$\begin{aligned}
C_{4,2} = & -\frac{2}{9} \frac{\cosh(h)}{\sinh^3(h) \left(2 \cosh^2(h) \hat{P}_1 - \cosh^2(h) \hat{P}_2 + \cosh^2(h) - \hat{P}_1 - 1\right)^2 \left(\left(8 + 12\hat{P}_1 - 4\hat{P}_3\right) \cosh^2(h) - 8 - 9\hat{P}_1 + \hat{P}_3\right)} \\
& \times \left(-\frac{64\hat{P}_1|\hat{P}_1+1|}{3} \left(\left(\frac{5|\hat{P}_1|^2}{16} \left(\frac{7}{20} + \hat{P}_1^3 + \left(-\frac{13\hat{P}_2}{20} - \frac{2}{15}\hat{P}_3 \right) \hat{P}_1^2 - 1/20 \left(\hat{P}_2 - \frac{13}{3}\hat{P}_3 \right) \hat{P}_2\hat{P}_1 - \frac{1}{30}\hat{P}_2^2\hat{P}_3 + \frac{133\hat{P}_1^2}{60} \right. \right. \right. \right. \\
& + \left. \left(-\frac{71\hat{P}_2}{60} - \frac{1}{20}\hat{P}_3 \right) P_1 - \frac{1}{12} \left(\hat{P}_2 - \frac{9}{5}\hat{P}_3 \right) P_2 + \frac{8}{5}\hat{P}_1 - \frac{3}{5}\hat{P}_2 + \frac{1}{20}\hat{P}_3 \right) + \hat{P}_1 \left(\frac{13}{32} + \hat{P}_1 \left(\hat{P}_1^3 + \left(-\frac{51\hat{P}_2}{64} - \frac{7\hat{P}_3}{48} \right) \hat{P}_1^2 \right. \right. \\
& + \left. \left. \frac{1}{32} \left(\hat{P}_2 + 17/2\hat{P}_3 \right) \hat{P}_2\hat{P}_1 - \frac{11\hat{P}_2^2\hat{P}_3}{192} \right) + \frac{647\hat{P}_1^3}{192} + \left(-\frac{145\hat{P}_2}{64} - \frac{41\hat{P}_3}{192} \right) \hat{P}_1^2 - \frac{\hat{P}_2\hat{P}_1}{96} \left(\hat{P}_2 - \frac{93\hat{P}_3}{2} \right) - \frac{13\hat{P}_2^2\hat{P}_3}{192} + \frac{799\hat{P}_1^2}{192} \right. \\
& + \left. \left(-\frac{71\hat{P}_2}{32} + \hat{P}_3/48 \right) \hat{P}_1 - \frac{5\hat{P}_2}{96} \left(\hat{P}_2 - \frac{19\hat{P}_3}{5} \right) - \frac{37\hat{P}_2}{48} + \frac{53\hat{P}_1}{24} + \frac{5\hat{P}_3}{64} \right) \cosh^{10}(h) + \left(-\frac{23|\hat{P}_1|^2}{32} \left(\frac{125}{276} + \hat{P}_1^3 \right. \right. \\
& + \left. \left. \left(-\frac{99\hat{P}_2}{184} - \frac{25\hat{P}_3}{138} \right) \hat{P}_1^2 + \frac{13\hat{P}_2\hat{P}_1}{184} \left(\hat{P}_2 + \frac{67\hat{P}_3}{39} \right) - \frac{11\hat{P}_2^2\hat{P}_3}{552} + \frac{1259\hat{P}_1^2}{552} + \left(-\frac{449\hat{P}_2}{552} - \frac{133\hat{P}_3}{552} \right) \hat{P}_1 + \frac{7\hat{P}_2}{138} \left(\hat{P}_2 + \frac{45\hat{P}_3}{28} \right) \right. \\
& + \left. \frac{121\hat{P}_1}{69} - \frac{29\hat{P}_2}{92} - \frac{11\hat{P}_3}{138} \right) - \frac{191P_1}{64} \left(\frac{239}{573} + \left(\hat{P}_1^3 + \left(-\frac{603\hat{P}_2}{764} - \frac{44\hat{P}_3}{191} \right) P_1^2 + \frac{123\hat{P}_2\hat{P}_1}{764} \left(\hat{P}_2 + \frac{161\hat{P}_3}{123} \right) - \frac{101\hat{P}_2^2\hat{P}_3}{2292} \right) \hat{P}_1 \right. \\
& + \left. \frac{2461\hat{P}_1^3}{764} + \left(-\frac{1501\hat{P}_2}{764} - \frac{1201\hat{P}_3}{2292} \right) \hat{P}_1^2 + \frac{169\hat{P}_2\hat{P}_1}{573} \left(\hat{P}_2 + \frac{831\hat{P}_3}{676} \right) - \frac{28\hat{P}_2^2\hat{P}_3}{573} + \frac{2213\hat{P}_1^2}{573} + \left(-\frac{303\hat{P}_2}{191} - \frac{71\hat{P}_3}{191} \right) \hat{P}_1 \right. \\
& + \left. \frac{74\hat{P}_2}{573} \left(\hat{P}_2 + \frac{163\hat{P}_3}{148} \right) + \frac{394\hat{P}_1}{191} - \frac{241\hat{P}_2}{573} - \frac{95\hat{P}_3}{1146} \right) \cosh^8(h) + \left(\frac{139|\hat{P}_1|^2}{256} \left(\frac{232}{417} + \hat{P}_1^3 + \left(-\frac{58\hat{P}_2}{139} - \frac{65\hat{P}_3}{417} \right) \hat{P}_1^2 \right. \right.
\end{aligned}$$

$$\begin{aligned}
& + \frac{12\hat{P}_2\hat{P}_1}{139} \left(\hat{P}_2 + \frac{7\hat{P}_3}{12} \right) - \frac{\hat{P}_2^2\hat{P}_3}{139} + \frac{1012\hat{P}_1^2}{417} + \left(-\frac{85\hat{P}_2}{139} - \frac{109\hat{P}_3}{417} \right) \hat{P}_1 + \frac{11\hat{P}_2}{139} \left(\hat{P}_2 + \frac{5\hat{P}_3}{11} \right) + \frac{830P_1}{417} - \frac{29\hat{P}_2}{139} - \frac{47\hat{P}_3}{417} \\
& + \frac{925\hat{P}_1}{256} \left(\frac{244}{555} + \left(\hat{P}_1^3 + \left(-\frac{583\hat{P}_2}{925} - \frac{213\hat{P}_3}{925} \right) \hat{P}_1^2 + \frac{99\hat{P}_2P_1}{925} \left(\hat{P}_2 + \frac{340\hat{P}_3}{297} \right) - \frac{12\hat{P}_2^2\hat{P}_3}{925} \right) \hat{P}_1 + \frac{3043\hat{P}_1^3}{925} + \left(-\frac{4487\hat{P}_2}{2775} \right. \right. \\
& \left. \left. - \frac{1642\hat{P}_3}{2775} \right) \hat{P}_1^2 + \frac{198\hat{P}_2\hat{P}_1}{925} \left(\hat{P}_2 + \frac{629\hat{P}_3}{594} \right) - \frac{13\hat{P}_2^2\hat{P}_3}{925} + \frac{2227\hat{P}_1^2}{555} + \left(-\frac{3706\hat{P}_2}{2775} - \frac{1382\hat{P}_3}{2775} \right) \hat{P}_1 + \frac{98\hat{P}_2}{925} \left(\hat{P}_2 + \frac{283\hat{P}_3}{294} \right) \\
& + \frac{6004\hat{P}_1}{2775} - \frac{974\hat{P}_2}{2775} - \frac{382\hat{P}_3}{2775} \left. \right) \cosh^6(h) - \frac{(1005\hat{P}_1 + 1005) \cosh^4(h)}{512} \left(\frac{21|\hat{P}_1|^2}{335} \left(\frac{37}{63} + \hat{P}_1^2 + \left(-\frac{13\hat{P}_2}{42} - \frac{11\hat{P}_3}{63} \right) P_1 \right. \right. \\
& \left. \left. + \frac{1}{14} \hat{P}_2\hat{P}_3 + \frac{191\hat{P}_1}{126} - \frac{5\hat{P}_2}{21} - \frac{13\hat{P}_3}{126} \right) + \hat{P}_1 \left(\frac{178}{335} + \hat{P}_1 \left(\hat{P}_1^2 + \left(-\frac{249\hat{P}_2}{670} - \frac{563\hat{P}_3}{3015} \right) \hat{P}_1 + \frac{319\hat{P}_2\hat{P}_3}{6030} \right) + \frac{15101\hat{P}_1^2}{6030} \right. \right. \\
& \left. \left. + \left(-\frac{428\hat{P}_2}{603} - \frac{1999\hat{P}_3}{6030} \right) \hat{P}_1 + \frac{173\hat{P}_2\hat{P}_3}{3015} + \frac{6124\hat{P}_1}{3015} - \frac{1006\hat{P}_2}{3015} - \frac{47\hat{P}_3}{335} \right) \right) + \frac{(311\hat{P}_1 + 311) \cosh^2(h)}{1024} \left(-\frac{19|\hat{P}_1|^2}{311} \left(\frac{65}{57} \right. \right. \\
& \left. \left. + \hat{P}_1^2 + \frac{11\hat{P}_1\hat{P}_3}{57} - \frac{1}{19} P_2\hat{P}_3 + \frac{125\hat{P}_1}{57} - \frac{\hat{P}_2}{19} + \frac{8P_3}{57} \right) + \hat{P}_1 \left(\frac{770}{933} + \left(P_1^2 + \left(\frac{9\hat{P}_2}{311} - \frac{113\hat{P}_3}{933} \right) \hat{P}_1 - \frac{4\hat{P}_2\hat{P}_3}{311} \right) \hat{P}_1 \right. \right. \\
& \left. \left. + \frac{2656\hat{P}_1^2}{933} + \left(\frac{14\hat{P}_2}{311} - \frac{83\hat{P}_3}{311} \right) \hat{P}_1 - \frac{3\hat{P}_2\hat{P}_3}{311} + \frac{830\hat{P}_1}{311} + \frac{6\hat{P}_2}{311} - \frac{133\hat{P}_3}{933} \right) \right) + \frac{87(\hat{P}_1 + 1)^2}{2048} \left(\frac{5|\hat{P}_1|^2}{29} \left(\frac{46}{45} + \hat{P}_1 + \frac{P_3}{45} \right) \right. \\
& \left. \left. + \hat{P}_1 \left(\frac{260}{261} + \left(\hat{P}_1 - \frac{47\hat{P}_3}{261} \right) \hat{P}_1 + \frac{520\hat{P}_1}{261} - \frac{46\hat{P}_3}{261} \right) \right) \right) + \frac{\cosh^{10}(h)}{1728} \left(1152 \left(\frac{7}{18} + \hat{P}_1^3 + \left(-\frac{7\hat{P}_2}{12} - \frac{\hat{P}_3}{9} \right) \hat{P}_1^2 - \frac{1}{12} \left(P_2 \right. \right. \right. \\
& \left. \left. \left. - \frac{7}{3} \hat{P}_3 \right) \hat{P}_2\hat{P}_1 - \frac{1}{36} \hat{P}_2^2\hat{P}_3 + \frac{83\hat{P}_1^2}{36} + \left(-\frac{41\hat{P}_2}{36} - \frac{\hat{P}_3}{36} \right) \hat{P}_1 - \frac{1}{9} \left(\hat{P}_2 - \frac{5}{4} \hat{P}_3 \right) \hat{P}_2 + \frac{31\hat{P}_1}{18} - \frac{11\hat{P}_2}{18} + \frac{\hat{P}_3}{18} \right) |\hat{P}_1|^4 \right.
\end{aligned}$$

$$\begin{aligned}
& + 36288 \left(\frac{200}{567} + \left(\hat{P}_1^3 + \left(-\hat{P}_3/7 - \frac{44\hat{P}_2}{63} \right) \hat{P}_1^2 - \frac{1}{42} \left(-\frac{88\hat{P}_3}{9} + \hat{P}_2 \right) \hat{P}_2 \hat{P}_1 - \frac{5\hat{P}_2^2 \hat{P}_3}{126} \right) \hat{P}_1 + \frac{29\hat{P}_1^3}{9} + \left(-\frac{368\hat{P}_2}{189} \right. \right. \\
& \left. \left. - \frac{115\hat{P}_3}{567} \right) \hat{P}_1^2 - \frac{5\hat{P}_2 \hat{P}_1}{54} \left(P_2 - \frac{452\hat{P}_3}{105} \right) - \frac{47\hat{P}_2^2 \hat{P}_3}{1134} + \frac{4345\hat{P}_1^2}{1134} + \left(-\frac{152\hat{P}_2}{81} - \frac{5\hat{P}_3}{1134} \right) \hat{P}_1 - \frac{40\hat{P}_2}{567} \left(\hat{P}_2 - \frac{23\hat{P}_3}{10} \right) \right. \\
& \left. + \frac{2227\hat{P}_1}{1134} - \frac{358\hat{P}_2}{567} + \frac{61\hat{P}_3}{1134} \right) \hat{P}_1 |\hat{P}_1|^2 + 1728\hat{P}_1^2 \left(\frac{166}{27} + \left(\hat{P}_1 - 4\hat{P}_2 \right) \left(\hat{P}_1 - \frac{\hat{P}_3}{3} \right) \hat{P}_1^2 \left(\hat{P}_1 - \frac{\hat{P}_2}{2} \right) + \frac{127\hat{P}_1}{6} \left(\hat{P}_1^3 \right. \right. \\
& \left. \left. + \left(-\frac{163\hat{P}_2}{127} - \frac{17\hat{P}_3}{127} \right) \hat{P}_1^2 + \frac{\left(29\hat{P}_2 + \frac{145\hat{P}_3}{3} \right) \hat{P}_2 P_1}{127} - \frac{13\hat{P}_2^2 \hat{P}_3}{127} \right) + \frac{367\hat{P}_1^3}{6} + \left(-\frac{157\hat{P}_2}{3} - \frac{127\hat{P}_3}{54} \right) \hat{P}_1^2 + \frac{25\hat{P}_2 P_1}{9} \left(\frac{272\hat{P}_3}{75} \right. \right. \\
& \left. \left. + \hat{P}_2 \right) - \frac{41\hat{P}_2^2 \hat{P}_3}{27} + \frac{3767\hat{P}_1^2}{54} + \left(-\frac{1156\hat{P}_2}{27} + \frac{95\hat{P}_3}{54} \right) \hat{P}_1 - \frac{2\hat{P}_2 \left(-47\hat{P}_3 + \hat{P}_2 \right)}{27} + \frac{943\hat{P}_1}{27} - \frac{356\hat{P}_2}{27} + \frac{43\hat{P}_3}{27} \right) \\
& + \frac{\cosh^8(h)}{1728} \left(-2496 \left(\frac{79}{156} + \hat{P}_1^3 + \left(-\frac{49\hat{P}_2}{104} - \frac{2}{13} P_3 \right) \hat{P}_1^2 + \frac{5\hat{P}_2 \hat{P}_1}{104} \left(\hat{P}_2 + \frac{31\hat{P}_3}{15} \right) - \frac{5\hat{P}_2^2 \hat{P}_3}{312} + \frac{19\hat{P}_1^2}{8} + \left(-\frac{233\hat{P}_2}{312} \right. \right. \right. \\
& \left. \left. - \frac{5\hat{P}_3}{24} \right) \hat{P}_1 + \frac{5\hat{P}_2}{156} \left(\hat{P}_2 + \frac{21\hat{P}_3}{10} \right) + \frac{74\hat{P}_1}{39} - \frac{4\hat{P}_2}{13} - \frac{11\hat{P}_3}{156} \right) |\hat{P}_1|^4 - 90576 \left(\frac{2432}{5661} + \left(\hat{P}_1^3 + \left(-\frac{383\hat{P}_3}{1887} - \frac{389\hat{P}_2}{629} \right) \hat{P}_1^2 \right. \right. \\
& \left. \left. + \frac{63\hat{P}_2 \hat{P}_1}{629} \left(\frac{283\hat{P}_3}{189} + \hat{P}_2 \right) - \frac{1}{37} \hat{P}_2^2 \hat{P}_3 \right) \hat{P}_1 + \frac{2034\hat{P}_1^3}{629} + \left(-\frac{963\hat{P}_2}{629} - \frac{294\hat{P}_3}{629} \right) \hat{P}_1^2 + \frac{332\hat{P}_2 \hat{P}_1}{1887} \left(\hat{P}_2 + \frac{1423\hat{P}_3}{996} \right) \right. \\
& \left. - \frac{158\hat{P}_2^2 \hat{P}_3}{5661} + \frac{7391\hat{P}_1^2}{1887} + \left(-\frac{7076\hat{P}_2}{5661} - \frac{1967\hat{P}_3}{5661} \right) \hat{P}_1 + \frac{424\hat{P}_2}{5661} \left(\hat{P}_2 + \frac{141\hat{P}_3}{106} \right) + \frac{11965\hat{P}_1}{5661} - \frac{640\hat{P}_2}{1887} - \frac{475\hat{P}_3}{5661} \right) \hat{P}_1 |\hat{P}_1|^2 \\
& - 28080 \left(\frac{2092}{1755} + \hat{P}_1^2 \left(\hat{P}_1^3 + \left(-\frac{213\hat{P}_2}{130} - \frac{21\hat{P}_3}{65} \right) \hat{P}_1^2 + \frac{57\hat{P}_2 \hat{P}_1}{130} \left(\hat{P}_2 + \frac{65\hat{P}_3}{57} \right) - \frac{49\hat{P}_2^2 \hat{P}_3}{390} \right) + \frac{2443\hat{P}_1}{390} \left(\hat{P}_1^3 + \left(-\frac{2797\hat{P}_2}{2443} \right. \right. \right. \\
& \left. \left. - \frac{1693\hat{P}_3}{7329} \right) \hat{P}_1^2 + \frac{590\hat{P}_2 \hat{P}_1}{2443} \left(\hat{P}_2 + \frac{2027\hat{P}_3}{1770} \right) - \frac{132\hat{P}_2^2 \hat{P}_3}{2443} \right) + \frac{7859\hat{P}_1^3}{585} + \left(-\frac{6346\hat{P}_2}{585} - \frac{1204\hat{P}_3}{585} \right) \hat{P}_1^2 + \frac{952\hat{P}_2 \hat{P}_1}{585} \left(\frac{1579\hat{P}_3}{1428} \right.
\end{aligned}$$

$$\begin{aligned}
& + \hat{P}_2) - \frac{376\hat{P}_2^2\hat{P}_3}{1755} + \frac{2602\hat{P}_1^2}{195} + \left(-\frac{12094\hat{P}_2}{1755} - \frac{2011\hat{P}_3}{1755} \right) \hat{P}_1 + \frac{968\hat{P}_2}{1755} \left(\frac{45P_3}{44} + \hat{P}_2 \right) + \frac{11174\hat{P}_1}{1755} - \frac{308\hat{P}_2}{195} - \frac{374\hat{P}_3}{1755} \Big) \hat{P}_1^2 \Big) \\
& + \frac{\cosh^6(h)}{1728} \left(1656 \left(\frac{44}{69} + \hat{P}_1^3 + \left(-\frac{8\hat{P}_2}{23} - \frac{25\hat{P}_3}{207} \right) \hat{P}_1^2 + 2/23 \left(\hat{P}_2 + \frac{5\hat{P}_3}{18} \right) \hat{P}_2 P_1 - \frac{\hat{P}_2^2\hat{P}_3}{207} + \frac{524\hat{P}_1^2}{207} + \left(-\frac{103\hat{P}_2}{207} - \frac{5\hat{P}_3}{23} \right) \hat{P}_1 \right. \right. \\
& + \frac{17\hat{P}_2}{207} \left(\hat{P}_2 + \frac{3\hat{P}_3}{17} \right) + \frac{50\hat{P}_1}{23} - \frac{11P_2}{69} - \frac{7\hat{P}_3}{69} \Big) |\hat{P}_1|^4 + 81072\hat{P}_1 \left(\frac{838}{1689} + \hat{P}_1 \left(\hat{P}_1^3 + \left(-\frac{319\hat{P}_3}{1689} - \frac{569\hat{P}_2}{1126} \right) \hat{P}_1^2 \right. \right. \\
& + \frac{105P_2\hat{P}_1}{1126} \left(\frac{13\hat{P}_3}{15} + \hat{P}_2 \right) - \frac{11\hat{P}_2^2\hat{P}_3}{1126} \Big) + \frac{11305\hat{P}_1^3}{3378} + \left(-\frac{711\hat{P}_2}{563} - \frac{4973\hat{P}_3}{10134} \right) \hat{P}_1^2 + \frac{203\hat{P}_2\hat{P}_1}{1126} \left(\hat{P}_2 + \frac{50\hat{P}_3}{63} \right) - \frac{101\hat{P}_2^2\hat{P}_3}{10134} \\
& + \frac{42511\hat{P}_1^2}{10134} + \left(-\frac{10349\hat{P}_2}{10134} - \frac{477\hat{P}_3}{1126} \right) \hat{P}_1 + \frac{440\hat{P}_2}{5067} \left(\hat{P}_2 + \frac{57\hat{P}_3}{80} \right) + \frac{1320\hat{P}_1}{563} - \frac{446\hat{P}_2}{1689} - \frac{206\hat{P}_3}{1689} \Big) |\hat{P}_1|^2 + 76248 \left(\frac{248}{353} \right. \\
& + \left(\hat{P}_1^3 + \left(-\frac{287\hat{P}_2}{353} - \frac{103\hat{P}_3}{353} \right) \hat{P}_1^2 + \frac{45\hat{P}_2\hat{P}_1}{353} \left(\hat{P}_2 + \frac{194P_3}{135} \right) - \frac{6\hat{P}_2^2\hat{P}_3}{353} \right) \hat{P}_1^2 + \frac{5251\hat{P}_1}{1059} \left(\hat{P}_1^3 + \left(-\frac{3549\hat{P}_2}{5251} - \frac{3764\hat{P}_3}{15753} \right) \hat{P}_1^2 \right. \\
& + \frac{492\hat{P}_2\hat{P}_1}{5251} \left(\hat{P}_2 + \frac{637\hat{P}_3}{492} \right) - \frac{47\hat{P}_2^2\hat{P}_3}{5251} \Big) + \frac{29953\hat{P}_1^3}{3177} + \left(-\frac{5224\hat{P}_2}{1059} - \frac{16558\hat{P}_3}{9531} \right) \hat{P}_1^2 + \frac{190\hat{P}_2\hat{P}_1}{353} \left(\frac{1207\hat{P}_3}{1026} + \hat{P}_2 \right) - \frac{262\hat{P}_2^2\hat{P}_3}{9531} \\
& \frac{82838\hat{P}_1^2}{9531} + \left(-\frac{29362\hat{P}_2}{9531} - \frac{1162\hat{P}_3}{1059} \right) P_1 + \frac{1916\hat{P}_2}{9531} \left(\frac{1023\hat{P}_3}{958} + \hat{P}_2 \right) + \frac{4156\hat{P}_1}{1059} - \frac{2180P_2}{3177} - \frac{268\hat{P}_3}{1059} \Big) \hat{P}_1^2 \Big) \\
& - \frac{(603\hat{P}_1 + 603) \cosh^4(h)}{16} \left(\frac{17|\hat{P}_1|^4}{5427} \left(2/3 + \hat{P}_1^2 + \left(-\frac{9\hat{P}_2}{34} - \frac{3\hat{P}_3}{17} \right) \hat{P}_1 + \frac{11\hat{P}_2\hat{P}_3}{102} + \frac{53\hat{P}_1}{34} - \frac{8\hat{P}_2}{51} - \frac{7\hat{P}_3}{102} \right) \right. \\
& + \frac{796\hat{P}_1|\hat{P}_1|^2}{1809} \left(\hat{P}_1 \left(\hat{P}_1^2 + \left(-\frac{277\hat{P}_2}{796} - \frac{36\hat{P}_3}{199} \right) \hat{P}_1 + \frac{143\hat{P}_2\hat{P}_3}{2388} \right) + \frac{5935\hat{P}_1^2}{2388} + \left(-\frac{382\hat{P}_2}{597} - \frac{727\hat{P}_3}{2388} \right) \hat{P}_1 + \frac{110\hat{P}_2\hat{P}_3}{1791} \right.
\end{aligned}$$

$$\begin{aligned}
& + \frac{2417\hat{P}_1}{1194} - \frac{520\hat{P}_2}{1791} - \frac{437\hat{P}_3}{3582} + \frac{968}{1791} \Big) + \hat{P}_1^2 \left(\frac{11668}{16281} + \left(\hat{P}_1^2 + \left(-\frac{343\hat{P}_3}{1809} - \frac{151\hat{P}_2}{402} \right) \hat{P}_1 + \frac{167\hat{P}_2\hat{P}_3}{3618} \right) \hat{P}_1^2 + \frac{4673\hat{P}_1}{1206} \left(\hat{P}_1^2 \right. \right. \\
& + \left. \left. \left(-\frac{1488\hat{P}_2}{4673} - \frac{2179\hat{P}_3}{14019} \right) \hat{P}_1 + \frac{1288\hat{P}_2\hat{P}_3}{42057} \right) + \frac{29528\hat{P}_1^2}{5427} + \left(-\frac{7138\hat{P}_2}{5427} - \frac{3310\hat{P}_3}{5427} \right) \hat{P}_1 + \frac{1186\hat{P}_2\hat{P}_3}{16281} + \frac{5938\hat{P}_1}{1809} - \frac{7436\hat{P}_2}{16281} \right. \\
& \left. - \frac{3206\hat{P}_3}{16281} \right) \Big) + \frac{(265\hat{P}_1 + 265) \cosh^2(h)}{32} \left(-\frac{7|\hat{P}_1|^4}{795} \left(\frac{67}{63} + \hat{P}_1^2 + \frac{1}{9}\hat{P}_1\hat{P}_3 - \frac{1}{21}\hat{P}_2\hat{P}_3 + \frac{19\hat{P}_1}{9} - \frac{\hat{P}_2}{21} + \frac{4\hat{P}_3}{63} \right) \right. \\
& + \frac{68\hat{P}_1|\hat{P}_1|^2}{795} \left(\left(\hat{P}_1^2 + \left(\frac{3\hat{P}_2}{68} - \frac{25\hat{P}_3}{51} \right) \hat{P}_1 + \frac{5\hat{P}_2\hat{P}_3}{204} \right) \hat{P}_1 + \frac{479\hat{P}_1^2}{204} + \left(\frac{23\hat{P}_2}{204} - \frac{599\hat{P}_3}{612} \right) \hat{P}_1 + \frac{7\hat{P}_2\hat{P}_3}{204} + \frac{1039\hat{P}_1}{612} + \frac{4\hat{P}_2}{51} \right. \\
& \left. - \frac{293\hat{P}_3}{612} + \frac{55}{153} \right) + \hat{P}_1^2 \left(\frac{7028}{7155} + \hat{P}_1^2 \left(\hat{P}_1^2 + \left(-\frac{61\hat{P}_3}{795} + \frac{9\hat{P}_2}{265} \right) \hat{P}_1 - \frac{4\hat{P}_2\hat{P}_3}{265} \right) + \frac{3214\hat{P}_1}{795} \left(\hat{P}_1^2 + \left(\frac{36\hat{P}_2}{1607} - \frac{685\hat{P}_3}{9642} \right) \hat{P}_1 \right. \right. \\
& \left. \left. - \frac{67\hat{P}_2\hat{P}_3}{9642} \right) + \frac{14468\hat{P}_1^2}{2385} + \left(\frac{194\hat{P}_2}{2385} - \frac{491\hat{P}_3}{1431} \right) \hat{P}_1 - \frac{2\hat{P}_2\hat{P}_3}{159} + \frac{28658\hat{P}_1}{7155} + \frac{4\hat{P}_2}{159} - \frac{946\hat{P}_3}{7155} \right) \Big) + \frac{3}{4} \left(\frac{1}{48} \left(\frac{10}{9} + \hat{P}_1 \right. \right. \\
& \left. \left. + \frac{\hat{P}_3}{9} \right) |\hat{P}_1|^4 + \frac{35\hat{P}_1|\hat{P}_1|^2}{48} \left(\hat{P}_1 \left(\hat{P}_1 - \frac{23\hat{P}_3}{315} \right) + \frac{125\hat{P}_1}{63} - \frac{\hat{P}_3}{15} + \frac{104}{105} \right) + \left(\frac{79}{54} + \hat{P}_1^2 \left(\hat{P}_1 - \frac{17\hat{P}_3}{72} \right) + \frac{503\hat{P}_1}{144} \left(\hat{P}_1 \right. \right. \right. \\
& \left. \left. - \frac{227\hat{P}_3}{1509} \right) + \frac{427\hat{P}_1}{108} - \frac{31\hat{P}_3}{108} \right) \hat{P}_1^2 \Big) \left(\hat{P}_1 + 1 \right)^2 \Big) \left(-\frac{2\hat{P}_1|\hat{P}_1 + 1|}{27} \left(2 \cosh^2(h) |\hat{P}_1|^2 + 18 \cosh^2(h) \hat{P}_1^2 - 2 \cosh^2(h) \hat{P}_1 \hat{P}_2 \right. \right. \\
& \left. \left. + 18 \cosh^2(h) \hat{P}_1 - |\hat{P}_1|^2 - 9\hat{P}_1^2 - 10\hat{P}_1 \right) + \frac{1}{162} \left(\left(2|\hat{P}_1|^4 + 108 \left(\hat{P}_1 - \hat{P}_2/27 + 1 \right) \hat{P}_1 |\hat{P}_1|^2 + 162\hat{P}_1^4 + \left(-36\hat{P}_2 \right. \right. \right. \right.
\end{aligned}$$

$$\left. + 396 \hat{P}_1^3 + (-40 \hat{P}_2 + 232) \hat{P}_1^2 \right) \cosh^2(h) - \frac{|\hat{P}_1|^4}{162} + \frac{(-54 \hat{P}_1^2 - 56 \hat{P}_1) |\hat{P}_1|^2}{162} - \frac{1}{2} \hat{P}_1^4 - \frac{4}{3} \hat{P}_1^3 - \frac{68 \hat{P}_1^2}{81} \right)^{-1} \tag{A 68}$$

REFERENCES

- ABLOWITZ, MARK J 2011 *Nonlinear dispersive waves: asymptotic analysis and solitons*, , vol. 47. Cambridge University Press.
- AL-ZANAIDI, M A & HUI, W H 1984 Turbulent airflow over water waves—a numerical study. *Journal of Fluid Mechanics* **148**, 225–246.
- BANNER, M L & MELVILLE, W K 1976 On the separation of air flow over water waves. *Journal of Fluid Mechanics* **77** (04), 825–842.
- BANNER, MICHAEL L & SONG, JIN-BAO 2002 On determining the onset and strength of breaking for deep water waves. part II: Influence of wind forcing and surface shear. *Journal of physical oceanography* **32** (9), 2559–2570.
- BELCHER, S E & HUNT, J C R 1993 Turbulent shear flow over slowly moving waves. *Journal of Fluid Mechanics* **251**, 109–148.
- BRUNETTI, MAURA & KASPARIAN, JÉRÔME 2014 Modulational instability in wind-forced waves. *Physics Letters A* **378** (48), 3626–3630.
- BRUNETTI, MAURA, MARCHIANDO, NADÈGE, BERTI, NICOLAS & KASPARIAN, JÉRÔME 2014 Nonlinear fast growth of water waves under wind forcing. *Physics Letters A* **378** (14–15), 1025–1030.
- BUCKLEY, MARC P & VERON, FABRICE 2016 Structure of the airflow above surface waves. *Journal of Physical Oceanography* **46** (5), 1377–1397.
- BUCKLEY, MARC P & VERON, FABRICE 2017 Airflow measurements at a wavy air–water interface using piv and lif. *Experiments in Fluids* **58** (11), 161.
- BUCKLEY, M P & VERON, F 2019 The turbulent airflow over wind generated surface waves. *European Journal of Mechanics-B/Fluids* **73**, 132–143.
- COX, CHARLES & MUNK, WALTER 1956 Slopes of the sea surface deduced from photographs of sun glitter. *Bulletin of the Scripps Institution of Oceanography* **6** (9), 401–488.
- DEIKE, LUC, PIZZO, NICK & MELVILLE, W KENDALL 2017 Lagrangian transport by breaking surface waves. *Journal of Fluid Mechanics* **829**, 364–391.
- DONELAN, MARK A, BABANIN, ALEXANDER V, YOUNG, IAN R & BANNER, MICHAEL L 2006 Wave-follower field measurements of the wind-input spectral function. part II: Parameterization of the wind input. *Journal of Physical Oceanography* **36** (8), 1672–1689.
- DONELAN, MARK A, BABANIN, ALEXANDER V, YOUNG, IAN R, BANNER, MICHAEL L & MCCORMICK, CYRIL 2005 Wave-follower field measurements of the wind-input spectral function. part I: Measurements and calibrations. *Journal of Atmospheric and Oceanic Technology* **22** (7), 799–813.
- DRAKE, THOMAS G & CALANTONI, JOSEPH 2001 Discrete particle model for sheet flow sediment transport in the nearshore. *Journal of Geophysical Research: Oceans* **106** (C9), 19859–19868.
- ELGAR, STEVE, FREILICH, M H & GUZA, R T 1990 Model-data comparisons of moments of nonbreaking shoaling surface gravity waves. *Journal of Geophysical Research: Oceans* **95** (C9), 16055–16063.
- ELGAR, STEVE & GUZA, R T 1985 Observations of bispectra of shoaling surface gravity waves. *Journal of Fluid Mechanics* **161**, 425–448.
- ELGAR, STEVE & GUZA, R T 1986 Nonlinear model predictions of bispectra of shoaling surface gravity waves. *Journal of Fluid Mechanics* **167**, 1–18.
- FANG, CHUNG 2019 *An Introduction to Fluid Mechanics*. Springer.
- FEDDERSEN, FALK & VERON, FABRICE 2005 Wind effects on shoaling wave shape. *Journal of physical oceanography* **35** (7), 1223–1228.
- GENT, P R & TAYLOR, P A 1976 A numerical model of the air flow above water waves. *Journal of Fluid Mechanics* **77** (1), 105–128.
- GONZALEZ-RODRIGUEZ, DAVID & MADSEN, OLE SECHER 2007 Seabed shear stress and bedload transport due to asymmetric and skewed waves. *Coastal Engineering* **54** (12), 914–929.
- GRASSO, FLORENT, MICHALLET, HERVÉ & BARTHÉLEMY, ERIC 2011 Sediment transport associated with morphological beach changes forced by irregular asymmetric, skewed waves. *Journal of Geophysical Research: Oceans* **116** (C3).
- HAO, XUANTING, CAO, TAO, YANG, ZIXUAN, LI, TIANYI & SHEN, LIAN 2018 Simulation-based study of wind-wave interaction. *Procedia IUTAM* **26** (1), 162–173.

- HAO, XUANTING & SHEN, LIAN 2019 Wind–wave coupling study using les of wind and phase-resolved simulation of nonlinear waves. *Journal of Fluid Mechanics* **874**, 391–425.
- HARA, TETSU & SULLIVAN, PETER P 2015 Wave boundary layer turbulence over surface waves in a strongly forced condition. *Journal of Physical Oceanography* **45** (3), 868–883.
- HASSELMANN, KLAUS 1962 Bispectra of ocean waves. In *Proc. Symp. Time Series Analysis*, pp. 125–139. John Wiley.
- HASSELMANN, KLAUS, BARNETT, TP, BOUWS, E, CARLSON, H, CARTWRIGHT, DE, ENKE, K, EWING, JA, GIENAPP, H, HASSELMANN, DE, KRUSEMAN, P & OTHERS 1973 Measurements of wind-wave growth and swell decay during the joint north sea wave project (jonswap). *Ergänzungsheft 8-12*.
- HAYNE, G 1980 Radar altimeter mean return waveforms from near-normal-incidence ocean surface scattering. *IEEE Transactions on Antennas and Propagation* **28** (5), 687–692.
- HOEFEL, FERNANDA & ELGAR, STEVE 2003 Wave-induced sediment transport and sandbar migration. *Science* **299** (5614), 1885–1887.
- HSU, TIAN-JIAN & HANES, DANIEL M 2004 Effects of wave shape on sheet flow sediment transport. *Journal of Geophysical Research: Oceans* **109** (C5).
- HUANG, NORDEN E, LONG, STEVEN R, TUNG, CHI-CHAO, YUAN, YELI & BLIVEN, LARRY F 1983 A non-gaussian statistical model for surface elevation of nonlinear random wave fields. *Journal of Geophysical Research: Oceans* **88** (C12), 7597–7606.
- HUSAIN, NYLA T, HARA, TETSU, BUCKLEY, MARC P, YOUSEFI, KIANOOSH, VERON, FABRICE & SULLIVAN, PETER P 2019 Boundary layer turbulence over surface waves in a strongly forced condition: Les and observation. *Journal of Physical Oceanography* **49** (8), 1997–2015.
- JACKSON, FREDERICK C 1979 The reflection of impulses from a nonlinear random sea. *Journal of Geophysical Research: Oceans* **84** (C8), 4939–4943.
- JANSSEN, PETER 2004 *The interaction of ocean waves and wind*. Cambridge University Press.
- JANSSEN, PETER AEM 1982 Quasilinear approximation for the spectrum of wind-generated water waves. *Journal of Fluid Mechanics* **117**, 493–506.
- JEFFREYS, HAROLD 1925 On the formation of water waves by wind. *Proc. R. Soc. Lond. A* **107** (742), 189–206.
- JOHNSON, JOEL T & CAI, YONGYAO 2002 A theoretical study of sea surface up/down wind brightness temperature differences. *IEEE transactions on geoscience and remote sensing* **40** (1), 66–78.
- KENDALL, JAMES M 1970 The turbulent boundary layer over a wall with progressive surface waves. *Journal of Fluid Mechanics* **41** (2), 259–281.
- KHARIF, C, KRAENKEL, ROBERTO ANDRÉ, MANNA, M A & THOMAS, R 2010 The modulational instability in deep water under the action of wind and dissipation. *Journal of Fluid Mechanics* **664**, 138–149.
- KOMEN, G J, CAVALERI, L, DONELAN, M, HASSELMANN, K, HASSELMANN, S & JANSSEN, P A E M 1994 *Dynamics and Modelling of Ocean Waves*. Cambridge University Press.
- KUNKEE, D B & GASIEWSKI, A J 1997 Simulation of passive microwave wind direction signatures over the ocean using an asymmetric-wave geometrical optics model. *Radio Science* **32** (1), 59–78.
- LAMONT-SMITH, T & WASEDA, T 2008 Wind wave growth at short fetch. *Journal of Physical Oceanography* **38** (7), 1597–1606.
- LEBLANC, STÉPHANE 2007 Amplification of nonlinear surface waves by wind. *Physics of Fluids* **19** (10), 101705.
- LEYKIN, I A, DONELAN, M A, MELLEN, R H & MCLAUGHLIN, D J 1995 Asymmetry of wind waves studied in a laboratory tank. *Nonlinear Processes in Geophysics* **2** (3/4), 280–289.
- LIGHTHILL, M J 1962 Physical interpretation of the mathematical theory of wave generation by wind. *Journal of Fluid Mechanics* **14** (3), 385–398.
- LIU, YI, YANG, DI, GUO, XIN & SHEN, LIAN 2010 Numerical study of pressure forcing of wind on dynamically evolving water waves. *Physics of Fluids* **22** (4), 041704.
- LONGUET-HIGGINS, MICHAEL SELWYN 1962 The directional spectrum of ocean waves, and processes of wave generation. *Proceedings of the Royal Society of London. Series A. Mathematical and Physical Sciences* **265** (1322), 286–315.

- LONGUET-HIGGINS, MICHAEL S 1969 Action of a variable stress at the surface of water waves. *The Physics of Fluids* **12** (4), 737–740.
- MEI, C C, STIASSNIE, M & YUE, D K P 2005 *Theory and Applications of Ocean Surface Waves: Nonlinear aspects. Advanced series on ocean engineering* 2. World Scientific.
- MILES, JOHN W 1957 On the generation of surface waves by shear flows. *Journal of Fluid Mechanics* **3** (2), 185–204.
- MITSUYASU, H & HONDA, T 1982 Wind-induced growth of water waves. *Journal of Fluid Mechanics* **123**, 425–442.
- MONIN, A S & OBUKHOV, A M F 1954 Basic laws of turbulent mixing in the surface layer of the atmosphere. *Contrib. Geophys. Inst. Acad. Sci. USSR* **151** (163), e187.
- OBERHAGEMANN, JAN, LEY, JENS & EL MOCTAR, BETTAR OULD 2013 Prediction of ship response statistics in severe sea conditions using rans. In *ASME 2012 31st International Conference on Ocean, Offshore and Arctic Engineering*, pp. 583–593. American Society of Mechanical Engineers Digital Collection.
- ONORATO, MIGUEL & PROMENT, DAVIDE 2012 Approximate rogue wave solutions of the forced and damped nonlinear schrödinger equation for water waves. *Physics Letters A* **376** (45), 3057–3059.
- PEDERSEN, G 2006 Multiple scale methods.
- PHILLIPS, OWEN M 1957 On the generation of waves by turbulent wind. *J. Fluid Mech* **2** (5), 417–445.
- PIEPMEIER, JEFFREY R & GASIEWSKI, ALBIN J 2001 High-resolution passive polarimetric microwave mapping of ocean surface wind vector fields. *IEEE Transactions on Geoscience and Remote Sensing* **39** (3), 606–622.
- PLANT, W J & WRIGHT, J W 1977 Growth and equilibrium of short gravity waves in a wind-wave tank. *Journal of Fluid Mechanics* **82** (4), 767–793.
- SHEMDIN, OMAR H & HSU, EN YUN 1967 Direct measurement of aerodynamic pressure above a simple progressive gravity wave. *Journal of Fluid Mechanics* **30** (2), 403–416.
- SNYDER, RL 1966 A field study of the wind generation of ocean waves. *J. mar. Res.* **24**, 141–178.
- SOARES, GUEDES C, FONSECA, N & PASCOAL, R 2008 Abnormal wave-induced load effects in ship structures. *Journal of ship research* **52** (1), 30–44.
- STOKES, GEORGE G 1880 On the theory of oscillatory waves. *Transactions of the Cambridge Philosophical Society* .
- TAYLOR, PETER K & YELLAND, MARGARET J 2001 The dependence of sea surface roughness on the height and steepness of the waves. *Journal of physical oceanography* **31** (2), 572–590.
- TOLAND, J F 2000 On the symmetry theory for stokes waves of finite and infinite depth. *Trends in applications of mathematics to mechanics* **106**, 207–217.
- TROITSKAYA, YU I, SERGEEV, D A, KANDAUROV, A A, BAIDAKOV, G A, VDOVIN, M A & KAZAKOV, V I 2012 Laboratory and theoretical modeling of air-sea momentum transfer under severe wind conditions. *Journal of Geophysical Research: Oceans* **117** (C11).
- VERON, F, SAXENA, G & MISRA, S K 2007 Measurements of the viscous tangential stress in the airflow above wind waves. *Geophysical Research Letters* **34** (19).
- A DIVISION OF WATERLOO MAPLE INC., MAPLESOFT, 2018 Maple 2018. Waterloo, Ontario.
- WHITHAM, GERALD BERESFORD 2011 *Linear and nonlinear waves*, , vol. 42. John Wiley & Sons.
- XIE, ZHIHUA 2014 Numerical modelling of wind effects on breaking solitary waves. *European Journal of Mechanics-B/Fluids* **43**, 135–147.
- XIE, ZHIHUA 2017 Numerical modelling of wind effects on breaking waves in the surf zone. *Ocean Dynamics* **67** (10), 1251–1261.
- XUAN, ANQING ELLIOTT, DENG, BINGQING, CAO, TAO & SHEN, LIAN 2016 Numerical study on the effects of progressive gravity waves on turbulence. *Journal of Hydrodynamics, Ser. B* **28** (6), 1011–1017.
- YAN, S & MA, QW 2010 Numerical simulation of interaction between wind and 2d freak waves. *European Journal of Mechanics-B/Fluids* **29** (1), 18–31.
- YANG, DI, MENEVEAU, CHARLES & SHEN, LIAN 2013 Dynamic modelling of sea-surface roughness for large-eddy simulation of wind over ocean wavefield. *Journal of Fluid Mechanics* **726**, 62–99.

- YANG, DI & SHEN, LIAN 2009 Characteristics of coherent vortical structures in turbulent flows over progressive surface waves. *Physics of Fluids* **21** (12), 125106.
- YANG, DI & SHEN, LIAN 2010 Direct-simulation-based study of turbulent flow over various waving boundaries. *Journal of Fluid Mechanics* **650**, 131–180.
- YOUNG, IAN R 1999 *Wind generated ocean waves*, , vol. 2. Elsevier.
- YOUNG, W R & WOLFE, C L 2014 Generation of surface waves by shear-flow instability. *Journal of Fluid Mechanics* **739**, 276–307.